New strategies for mitigating the Grey Area in DDES models

A. Pont-Vílchez *
Universitat Politècnica de Catalunya, Terrassa, Spain, E-08222

A. Duben † and A. Gorobets ‡
Keldysh Institute of Applied Mathematics of Russian Academy of Sciences, Moscow, Russia, 125047

A. Revell §
University of Manchester, Manchester, United Kingdom, M13 9PL

A. Oliva ¶ and F.X. Trias‖
Universitat Politècnica de Catalunya, Terrassa, Spain, E-08222

This paper presents a new approach for mitigating the unphysical delay in the RANS to LES transition, often referred to as the *Grey Area*, which is a common issue for hybrid RANS-LES turbulence models such as Delayed-Detached Eddy Simulation (DDES). An existing methodology designed for improving the LES performance in complex flows is adapted and tested. This is based on reducing the numerical diffusion in critical areas for permitting a more accurate development of turbulence. The new formulation comprises both a 2D sensitive velocity gradient model and an alternative definition of the subgrid length scale, which are tested both individually and in tandem, and compared with the other formulations commonly used for addressing the *Grey Area*. Four test cases are examined, a flat plate, two variants of the incompressible backward facing step and an open jet compressible case; all of which are selected to expose the adverse impact of numerical diffusion which we seek to address. Furthermore, the proposed changes are implemented in two different codes for the purpose of cross-validation. Encouraging results are observed and examined via detailed analysis, supporting the suitability of the new approach as a candidate for addressing the *Grey Area* issue in flows of this kind.

Nomenclature

C_{sgs} = Subgrid scale constant in LES models

$D_{\text{sgs}}(\bar{\boldsymbol{u}})$ = Differential operator used in LES models

*PhD Student, Heat and Mass Transfer Transfer Technological Center (CTTC), arnau@cttc.upc.edu
†Researcher, Keldysh Institute of Applied Mathematics of Russian Academy of Sciences, alexey.duben@gmail.com
‡Leading Researcher, Keldysh Institute of Applied Mathematics of Russian Academy of Sciences, andrey.gorobets@gmail.com
§Reader, Department of Mechanical, Aerospace & Civil Engineering, alistair.revell@manchester.ac.uk
¶Professor, Heat and Mass Transfer Technological Center (CTTC), oliva@cttc.upc.edu
‖Associate Professor, Heat and Mass Transfer Technological Center (CTTC), xavi@cttc.upc.edu

$D^{2D}_{\text{sgs}}(\bar{\boldsymbol{u}})$	=	$D_{\text{sgs}}(\bar{\boldsymbol{u}})$ sensitive to 2D flows
G	=	Gradient velocity tensor
h	=	Step height of the Backward Facing Step
J	=	Jacobian tensor of the transformation from the physical space to the computational space
$\boldsymbol{l}$	=	r_n projected into the plane defined by $\boldsymbol{\omega}$
$\bar{p}$	=	Kinematic pressure filtered by a LES filter
P_{A}	=	First invariant of a second order tensor, A
Q_{A}	=	Second invariant of a second order tensor, A
R_{A}	=	Third invariant of a second order tensor, A
Re	=	Reynolds number
Re_τ	=	Friction Reynolds number
rms	=	Root mean square
sgs	=	Sub-grid scale
r_n	=	Distance from the center of the cell to one vertex
S	=	Rate-of-strain tensor
$\tilde{\mathsf{S}}$	=	Traceless part of S
U_{max}	=	Centerline velocity at the channel inflow
U_b	=	Bulk velocity at the channel inflow
$\boldsymbol{u}$	=	Velocity vector
$\bar{\boldsymbol{u}}$	=	Filtered by a LES filter
U_o	=	Center-line velocity at the Backward Facing Step inflow
U_{jet}	=	Center-line velocity at the Jet inflow
y^+	=	distance normal to the wall in wall units
β	=	Aspect ratio in a rectangular cell, $\Delta x/\Delta y$
Δ	=	Subgrid length scale scalar
$\boldsymbol{\Delta}$	=	Subgrid length scale tensor
Δ_{max}	=	Δ based on the max dimension in a structured cell
Δ_{lsq}	=	Least-square Δ
Δ_{SLA}	=	Shear layer adapted Δ
$\tilde{\Delta}_\omega$	=	Δ based on the largest cell dimension in the $\boldsymbol{\omega}$ plane
ν	=	Kinematic viscosity
ν_t	=	Turbulent kinematic viscosity

ν_{sgs} = Subgrid scale kinematic viscosity

τ = Kinematic subgrid stress tensor

ω = Vorticity vector

I. Introduction

During the last decades, numerical simulations have become an essential tool for every-day understanding and prediction of the flow behavior in industrial applications. Reynolds-Averaged Navier-Stokes (RANS) models have been, and continue to be, widely used due to their cost-effective nature. However, these methodologies do not perform well when unsteady data is required or when complex flow motions are involved. For covering such a purpose, other techniques such as Large Eddy Simulation (LES) are recommeneded. Unfortunately, its routine use usually requires a heavy amount of computational resources, so its use remains relatively scarce; limited to industrial sectors and research cases where extra accuracy requirements justify the additional expense. In this regard, a set of hybrid RANS-LES methodologies were specifically designed for circumventing the issues mentioned above. They were basically based on simulating the unsteady flow away from the wall using LES approaches, while managing the boundary layers close to the wall by means of RANS models.

In this context, DDES [1] is one of the most widely used hybrid models, due to its proven success in a range of applications where RANS becomes unreliable, such as massive flow separation. In contrast to the original version of Detached Eddy Simulation (DES) [2], the DDES non-zonal approach does not rely only on the mesh for defining the RANS and LES regions, but also on the flow field, by means of the shielding function, f_d. However, while some important weaknesses of the initial DES version where resolved, some others remain open. First, the flow separation due to adverse pressure gradient depends mainly on the underlying RANS model, with associated weaknesses and case dependency. The delayed development of the flow instabilities due the overly dissipative nature of RANS also contributes to the appearance of unphysical results. This is a numerical issue and is known colloquially as the Grey Area (*GA*) problem. The second problem concerns the balance of use of RANS and LES within the boundary layer. In general, a shielding function is introduced to the scheme to ensure that the attached boundary layer is modelled using RANS. Where this shielding is insufficient, the standard DES schemes tend to activate the LES model in a region which is insufficiently finely resolved by the grid, which in turn triggers an unphysical boundary layer physics and often flow separation. Recent studies [3–6] have focussed on the modification of DES-based schemes to improve this shielding. Menter [5] proposed the SBES (Stress Blended Eddy Simulation) method which adds a novel formulation to further protect the RANS boundary layer. Deck and Renard [6] also proposed a robust strategy for the RANS shielding of attached boundary layers in a hybrid RANS-LES methods that was demonstrated on a set of test cases. The present paper is focused on mitigating the first problem, diminishing the unphysical delay in the RANS to LES transition,

improving the accuracy of the resolved instabilities in such areas. The second problem has not been studied in detail, as all the methodologies compared in the paper presented similar properties close to the wall, indicating an acceptable performance of the standard shielding function [1]. However, these studies are clearly recommended for more complex flow configurations than those considered in this paper.

A good example of previous efforts to overcome the *GA* is the extensive work presented by Mockett et al. [7] where two different strategies were described. First, reducing the eddy-viscosity,

$$\nu_{\text{sgs}} = \left(C_{\text{sgs}}\Delta\right)^2 D_{\text{sgs}}\left(\bar{\boldsymbol{u}}\right), \tag{1}$$

in transition areas by either diminishing the Subgrid Length Scale (SLS), Δ, or the differential operators, $D_{\text{sgs}}\left(\bar{\boldsymbol{u}}\right)$, or both. Second, introducing artificial oscillations for triggering turbulence in the region of interest. Even though both strategies deal with the delay problem, the first one is preferable as it is consistent with the non-zonal DES ideology.

A number of other SLS definitions have been proposed by the DES community over the period since its inception (Δ_{max}). For instance, Chauvet et al. [8] introduced the concept of attributing a flow kinematic sensitivity to the SLS. In particular, they made Δ dependent on the vorticity vector. The formulation was subsequently generalized for unstructured meshes by Deck [9]. While results were promising in some cases this formulation led to unnecessarily small length scale in the near wall region, reducing the stability of RANS. Extending this idea further, Mockett et al. [7], proposed a new solution based on the flow kinematics,

$$\tilde{\Delta}_{\omega} = \frac{1}{\sqrt{3}} \max_{n,m=1,\ldots,8} |\boldsymbol{l}_n - \boldsymbol{l}_m|. \tag{2}$$

Where $\boldsymbol{l}$ is the distance from the center of the cell to one vertex r_n (n=1,. . . ,8 for hexahedral cell), projected into the plane defined by the vorticity vector, $\boldsymbol{\omega}$. In addition, various alternative differential operators were considered based on other LES models, aside from the classical Smagorinsky [10] (SMG). In particular, the $\sigma-$ LES [11] was selected as a good candidate for its ability to switch off in 2D flow regions. When both strategies ($\tilde{\Delta}_{\omega}$ and $\sigma-$ LES) were combined (also called $\sigma-$ DES), significant improvements were obtained with respect to the original DDES [1] at comparable computational cost [12, 13],

In addition, Shur et al. [14] proposed another SLS in combination with the SMG model,

$$\Delta_{\text{SLA}} = \tilde{\Delta}_{\omega} F_{KH}(\langle VTM \rangle), \tag{3}$$

where the $\tilde{\Delta}_{\omega}$ was modified to switch off in 2D flow regions through a blending function, $F_{KH}(\langle VTM \rangle)$. This strategy is known as the Shear Layer Adapted (SLA) approach. The Vortex Tilting Measure (VTM) coefficient is used as an

indicator of 2D flow regions,

$$VTM = \frac{|(\mathsf{S}\boldsymbol{\omega}) \times \boldsymbol{\omega}|}{\omega^2 \sqrt{-Q_{\tilde{\mathsf{S}}}}}. \tag{4}$$

Where the traceless part $\tilde{\mathsf{S}}$ of the rate-of-strain tensor, $\mathsf{S} = 1/2\left(\nabla\bar{\boldsymbol{u}} + \nabla\bar{\boldsymbol{u}}^T\right)$, is used. For incompressible flows, $\tilde{\mathsf{S}} = \mathsf{S}$ as the velocity field is divergence free. The second invariant of a second-order tensor A is defined as $Q_{\mathsf{A}} = 1/2(tr^2(\mathsf{A}) - tr(\mathsf{A}^2))$. The Δ_{SLA} was successfully applied to several flow configurations [13, 15], reducing the delay of the flow instabilities in the shear layer.

The objective of this paper, which is aligned with the σ − DES strategy, consists of exploring a recently developed LES strategy for mitigating the *GA* phenomenon. The hypothesis is that this numerical issue can be mitigated via the appropriate choice of SLS and $D_{\mathrm{sgs}}(\bar{\boldsymbol{u}})$ strategies. In this regard, the improvements suggested here are inherited from Trias et al. [16, 17], who developed a new family of LES models, $S3PQR$, and a new kinematic-sensitive SLS, Δ_{lsq}, based on the velocity gradient. They are explained in detail in the numerical approach in section II. While both approaches, $S3PQR$ and Δ_{lsq}, were originally designed and tested for LES applications, preliminar studies [18, 19] showed how they can be successfully applied to address the *GA* issue in DDES simulations.

In this paper, the performance of the new approach is compared to the existing methodologies described above ($SMG+\Delta_{\mathrm{SLA}}$ [14] and the σ − DES [12]). Δ_{vol}, a classic SLS for LES applications, has not been considered in the comparison due to its poor performance observed in previous works in the presence of anisotropic meshes (see [14, 17]). Four different flow configurations are considered: (i) the zero pressure gradient flat plate for studying the possible influence of the new approaches on the shielding function; (ii) the experimental results obtained by Vogel and Eaton [20] for an incompressible Backward Facing Step (BFS) at $\mathrm{Re}_h = 28000$ (based on inflow bulk velocity, U_b, and the step edge, h) and Expansion Ratio, $ER = 5/4$, a ratio of the outflow vs the input heights; (iii) the Direct Numerical Simulation (DNS) results of a BFS at $\mathrm{Re}_\tau = 395$ (based on the inlet conditions) and $ER = 2$ [21], where the growth of the Kelvin-Helmholtz instabilities in a shear layer is studied in detail and (iv) a compressible subsonic jet at $\mathrm{Re}_D = 1.1 \times 10^6$ and $M = 0.9$ [22, 23]. All these simulations have been carried out using two CFD codes, *OpenFOAM* and *NOISEtte* [24].

The rest of the paper is arranged as follows. In the next section, the new strategies proposed for mitigating the *GA* issue are defined. The cases used for studying the *GA* mitigation capabilities of the standard and new strategies are described in section III, as well as a short description of the two codes used in this work. The behavior of the new approach is compared with the standard mitigation techniques in section IV, using the cases and codes mentioned above. Finally, the main conclusions of this work are outlined.

II. Mathematical Methodologies

In the following section, we present a couple of new methodologies for mitigating the *GA* issue based on the reduction of the ν_{sgs} (see Eq. 1) in critical areas, either by altering Δ or $D_{\text{sgs}}(\bar{\boldsymbol{u}})$. The impact of such coefficients on the *GA* issue can be understood analyzing the DDES equations, as follows

$$\partial_t \bar{\boldsymbol{u}} + (\bar{\boldsymbol{u}} \cdot \nabla)\,\bar{\boldsymbol{u}} = -\nabla \bar{p} + \nu \nabla^2 \bar{\boldsymbol{u}} - \nabla \cdot \tau, \quad \nabla \cdot \bar{\boldsymbol{u}} = 0, \tag{5}$$

where the subgrid stress tensor, τ, is modeled giving rise to a non-linear coupling with the filtered velocity itself, i.e. to solve the closure problem via the Bousinesq hypothesis, as follows

$$\tau(\bar{\boldsymbol{u}}) = -\nu_{\text{sgs}} \left(\nabla \bar{\boldsymbol{u}} + \nabla \bar{\boldsymbol{u}}^T \right) = -2\nu_{\text{sgs}} \mathsf{S}. \tag{6}$$

In a DDES model, ν_{sgs} is modeled using different RANS (for instance the Spalart-Allmaras [1] model), and is tuned to reduce to LES away from the wall, where the LES assumptions are applicable. Noting that ν_{sgs} is defined by Eq. 1, the direct dependence of both Δ and $D_{\text{sgs}}(\bar{\boldsymbol{u}})$ is readily apparent.

Therefore, considering that *GA* is generally a result of an excessive diffusion coming from the turbulence model ν_{sgs}, a reduction of Δ^2 or $D_{\text{sgs}}(\bar{\boldsymbol{u}})$ in critical areas can be expected to bring a significant improvement to the overall simulation. In this context, techniques initially developed for improving the LES performance in complex flow configurations are introduced, exploring how they can contribute to address the *GA* issue in DDES simulations.

A. Subgrid Length Scales

The idea of considering the maximum meaningful scale of each control volume was explored by different authors, such as Mockett et al. [7], who developed $\tilde{\Delta}_\omega$ (Eq. 2). As a preview of ideas, we can analyse its performance for the following 2D simplified flow

$$\Delta = \begin{pmatrix} \Delta x & \\ & \Delta y \end{pmatrix} = \begin{pmatrix} \beta & \\ & \beta^{-1} \end{pmatrix}, \quad G = \begin{pmatrix} \partial_1 u_1 & \partial_2 u_1 \\ \partial_1 u_2 & \partial_2 u_2 \end{pmatrix} = \begin{pmatrix} 0 & 1 \\ 1-2\omega & 0 \end{pmatrix}, \tag{7}$$

where Δ is a diagonal matrix which represents the dimensions of the rectangular cell, the parameter β defines the aspect ratio ($\Delta x/\Delta y = \beta^2$) and G is the gradient velocity tensor. Results are displayed in figure 1, for a range of simple flow conditions ranging from pure shear ($\omega = 0$) to pure rotation ($\omega = 1$). Even though turbulence is a clearly 3D phenomenon, this 2D analysis helps to understand the most essential properties of each SLS. The Δ_{SLA} has not been included in this study as it sets to zero in 2D flows. Notice that the size of the control volume remains equal to unity (Eq. 7); therefore, $\Delta_{\text{vol}} = 1$, regardless of the value of β (where Δx is equal to β and Δy is β^{-1}). The effect of β

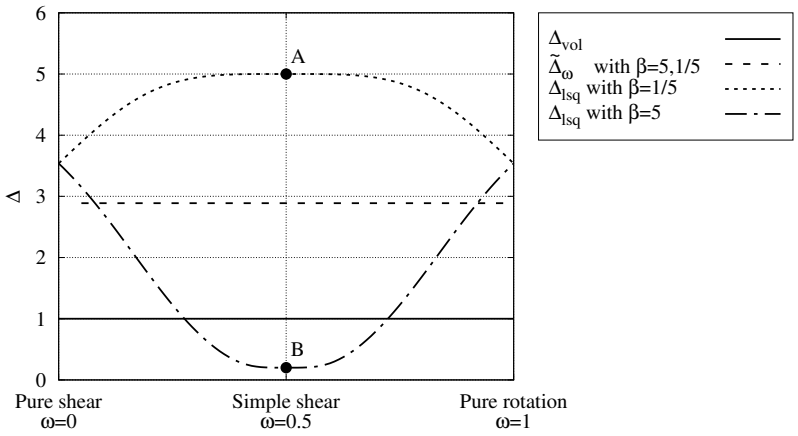

Fig. 1 Comparison between $\tilde{\Delta}_\omega$ and Δ_{lsq} for the simple 2D flow defined in Eq. 7 with different values of $\beta = 1/5, 1/2, 2, 5, 10$

into the cell's shape can be observed in figure 2. In a 2D motion $\tilde{\Delta}_\omega = \sqrt{\left(\beta^2 + \beta^{-2}\right)/3}$ only depends on the β ratio, but is not sensitive to either the flow behaviour or the volume rotation (the same results are obtained with $\beta = 5$ and $\beta = 1/5$). In the context of LES, Trias et al. [17] proposed a new SLS,

$$\Delta_{\text{lsq}} = \sqrt{\frac{\mathsf{JG}^T\mathsf{G} : \mathsf{JG}^T\mathsf{G}}{\mathsf{G}^T\mathsf{G} : \mathsf{G}^T\mathsf{G}}}, \mathsf{J} = \begin{pmatrix} \mathcal{J}_{ii}^x & & \\ & \mathcal{J}_{ii}^y & \\ & & \mathcal{J}_{ii}^z \end{pmatrix}, \mathcal{J}_{ii}^l = \frac{1}{\sum_{j!=i} \|G_{ij}^l\|}, \tag{8}$$

where J is the Jacobian of the transformation from the physical space to the computational space, which in a Cartesian structured and uniform mesh J becomes $diag(\Delta x, \Delta y, \Delta z)$. The components of the gradient tensor, G, in a specific direction, l, are represented by G_{ij}^l. It is worth to point out that G is actually being computed in any LES or DES code. This computationally inexpensive new SLS can be applied to structured or unstructured meshes, presenting a good resilience to spatial anisotropies. Its performance in a 2D flow is also presented in figure 1. In contrast to $\tilde{\Delta}_\omega$, Δ_{lsq} adapts to the flow behaviour and the cell orientation, providing completely different values in the simple shear ($\omega = 0.5$) case. In that situation, the spatial length scale is reduced to $\beta^{-1} = \Delta y$, priorising the direction with the highest gradient value (usually normal to the wall). This implies that, Δ_{lsq} could lead to erroneous results in the case of inconsistent refinement. However, it is usually not the case when Low-Re RANS models are used, as the refinement should be good enough to ensure a correct capture or the flow behaviour at the highest gradient regions (leading to meshes around $\Delta y^+ \approx 1$). The issues arise when High-Re RANS models are applied, since they employ wall functions in the near wall region and so extreme mesh refinement is no longer needed. In this situation, the use of Δ_{SLA} is apparently more appropriate, as the Δ would be deactivated in 2D flow region.

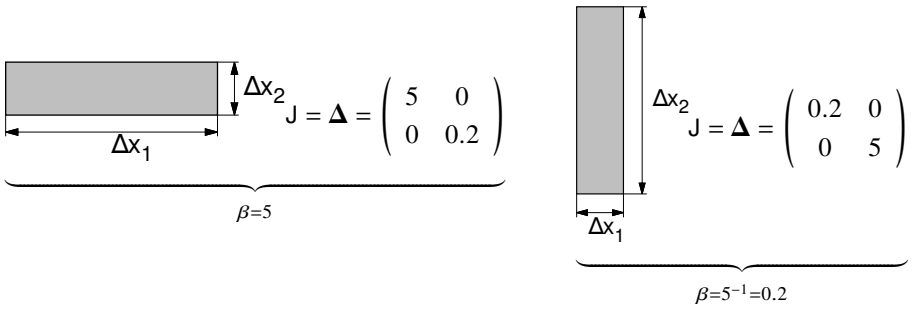

Fig. 2 An example showing how the cell's shape is affected by the β coefficient (5, 1/5). The cell volume is constant and equal to 1.

B. Turbulence Models

The possibility of considering other LES models in DDES applications was first studied by Mockett et al. [7]. The $\sigma-$LES model was proposed as a good candidate, due to its ability for switching off in 2D flow configurations and thus reducing the damping of shear layer instabilities. The same idea is shared at the core of the Δ_{SLA}, which was proposed by Shur et al. [14] as another Grey Area Mitigation (*GAM*) technique. These developments can be understood by the following reasoning:

$$\begin{aligned} \nu_{\mathrm{sgs}} &= \left(C_m \Delta_{\mathrm{SLA}}\right)^2 D_{\mathrm{sgs}}\left(\bar{\boldsymbol{u}}\right) \\ &= \left(C_m \tilde{\Delta}_{\omega}\right)^2 \left(F_{KH}(\langle VTM\rangle)^2 D_{\mathrm{sgs}}\left(\bar{\boldsymbol{u}}\right)\right) \\ &= \left(C_m \tilde{\Delta}_{\omega}\right)^2 D^{2D}_{\mathrm{sgs}}\left(\bar{\boldsymbol{u}}\right). \end{aligned} \tag{9}$$

where Δ_{SLA} is read as $\tilde{\Delta}_{\omega}$ coupled with an ex professo designed $D^{2D}_{\mathrm{sgs}}\left(\bar{\boldsymbol{u}}\right)$, providing 2D flow sensitivity to the differential opperator, $D_{\mathrm{sgs}}\left(\bar{\boldsymbol{u}}\right)$. The fact that $F_{KH}(\langle VTM\rangle)$ is a dimensionless function, helps and sustains the arguments raised above. However, we should also mention that modifying Δ has a direct impact in both the RANS and LES areas, whereas it is not the case for $D^{2D}_{\mathrm{sgs}}\left(\bar{\boldsymbol{u}}\right)$.

The present paper aims to study the effect of using $D^{2D}_{\mathrm{sgs}}\left(\bar{\boldsymbol{u}}\right)$ in the *GA*; applying LES models directly inherited from LES. In particular, we employ the familiy of LES models developed by Trias et al. [16],

$$D^{S3PQR}_{\mathrm{sgs}}\left(\bar{u}\right) = P^{p}_{\mathsf{G}\mathsf{G}^T} Q^{-(p+1)}_{\mathsf{G}\mathsf{G}^T} R^{(p+5/2)/3}_{\mathsf{G}\mathsf{G}^T}, \tag{10}$$

where $P_{\mathsf{A}} = tr(\mathsf{A})$, $Q_{\mathsf{A}} = 1/2(tr^2(\mathsf{A}) - tr(\mathsf{A}^2))$ and $R_{\mathsf{A}} = det(\mathsf{A})$ are the first, second and third invariants of a second-order tensor A, respectively. In this case, A is equal to $\mathsf{G}\mathsf{G}^T$ and G refers to the gradient of the resolved velocity field, $\mathsf{G} \equiv \nabla\bar{\boldsymbol{u}}$. $\mathsf{G}\mathsf{G}^T$ is proportional to the gradient model [25] given by the leading term of the Taylor series expansion of the kinematic subgrid stress tensor $\tau\left(\bar{\boldsymbol{u}}\right) = \left(\Delta^2/12\right)\mathsf{G}\mathsf{G}^T + O\left(\Delta^4\right)$. In addition to the deactivation in 2D flows for $p > -5/2$, these

models also present a proper near-wall behavior [11]. In this paper, p is set to zero to ensure the deactivation of the model in the 2D flow regions, thus removing dependency on the P invariant, leading to the $S3QR$ model. Other p values could be explored, but no significant improvements are expected.

We employ a similar modification of the DDES approach to overcome negative influence on the shielding function to that proposed by Mockett et al. [7] and applied to the WALE and σ models. This approach considers the substitution of the velocity gradient invariant in the Spalart-Allmaras (SA) [26] RANS model $S^*_{\mathrm{SA}} = \sqrt{\Omega_{ij}\Omega_{ij}}$ with the following

$$S^*_{\mathrm{sgs-DDES}} = S^*_{\mathrm{SA}} - f_d \mathrm{pos}(l_{\mathrm{SA}} - l_{\mathrm{LES}})(S^*_{\mathrm{SA}} - B_{\mathrm{sgs}} D_{\mathrm{sgs}}), \tag{11}$$

where the operator $\mathrm{pos}(a) = 0$ if $a \leq 0$ and $\mathrm{pos}(a) = 1$ otherwise, $B_{\mathrm{sgs}} = C^2_{\mathrm{sgs}}/C^2_{\mathrm{SMG}}$ (C_{sgs} is the constant of corresponding SGS model), l_{SA} is wall-distance, $l_{\mathrm{LES}} = C_{\mathrm{DES}}\Psi\Delta_{\mathrm{sgs}}$. $C_{\mathrm{DES}} = 0.65$ (for SA-based DES models) is the model constant calibrated to perform as the Smagorinsky model in case of homogeneous isotropic turbulence, Ψ is introduced to compensate the unwanted activity of low-Re terms in those areas where the DDES is having a LES-like behaviour [1]. Additionally, C_{d1} coefficient from f_d is set to 10 to improve the shielding capabilities when alternative subgrid scale models are applied, such as σ and/or S3QR (following the recommendations of the paper [27]).

III. Simulation Set-up

A set of four different flow configurations has been used to test the above-mentioned techniques, considering both incompressible and compressible flows. Moreover, the performance of the new SLS and differential operators has been tested with two different CFD codes, *OpenFOAM* and *NOISEtte*.

A. Cases

All cases used here are well-known in the DES community for assessing the impact of *GA* mitigation methods. They present free shear layer regions in simple geometrical configurations, where the impact of the model on the anticipated development of instabilities can be easily studied.

- **Zero pressure gradient flat plate**

  The turbulent subsonic ($M_\infty = 0.1$) flow over the flat plate is considered. Two Reynolds numbers characterizing the flow are examined: $\mathrm{Re} = 2 \cdot 10^4$ and $\mathrm{Re} = 10^6$. The computational domain for both cases is a rectangle with the sizes $L_x = 5$ in the streamwise and $L_y = 1$ in the wall-normal directions. The precomputed profiles of streamwise velocity u and modified turbulent viscosity $\tilde{\nu}$ with particular boundary layer thicknesses were imposed at the input boundary (at $x = 0$): $\delta_{0.99} = 0.5$ and $\delta_{0.99} = 0.2$ for $\mathrm{Re} = 2 \cdot 10^4$ and $\mathrm{Re} = 10^6$, respectively. The fine meshes that were built for these simulations follow the WMLES recommendations (based on the $\delta_{0.99}$ of boundary layer at the inflow): $\Delta_x = \delta_{0.99}/10$, $\Delta_z = \delta_{0.99}/20$, $\Delta^+_{y,1} \leq 1$, $\Delta^{\max}_y < \Delta_x$. Only one cell in the span-wise

direction was considered for the simulations.

- **BFS: Vogel & Eaton (*BFS-VE*)**

  This *BFS* configuration resembles the experimental study carried out by Vogel and Eaton [20] at $\mathrm{Re}_h = 28000$ and ER equal to $5/4$. The fluid is incompressible and the Re_τ at the inflow is around 2500. The computational domain, mesh and boundary conditions can be found in work by Spalart et al. [1]. This configuration is a reference case in the DDES literature for studying the RANS to LES transition downstream of the step-edge. Hereafter, this case is named *BFS-VE* .

- **Instabilities' growth at the shear layer (*BFS-DNS*)**

  As well as considering fluctuation intensity as a means for evaluating model capabilities in the RANS to LES transition region, in this case we may also use a *BFS* case to study the growth of these instabilities along the shear layer. The case reported by Pont-Vílchez et al. [21] covers both of these aspects in an incompressible *BFS* at $\mathrm{Re}_\tau = 395$ and $ER = 2.0$. Emphasis was placed downstream of the step-edge, where the shear layer instabilties appear. In the present work, the dimensions of the computational domain have been reduced respect to the reference DNS case, in order to resemble the *BFS-VE* domain. These are $24h \times 2h \times 2h$, in the stream-wise, wall-normal and span-wise directions, respectively. The inflow is located at $4h$ from the expansion. The origin of coordinates is placed at the step-edge. In order to assess the mesh resilience capabilities for different *GAM* approaches, three meshes has been selected. They propose different refinement levels in the stream-wise direction (free shear layer area) just downstream the step-edge, $x_1 = [0, h]$. In these meshes, a length equal to 8, 16 and 32 wall-units for the first grid cell after the step-edge is used, respectively. The rest of mesh parameters are kept constant. These are: the Poisson growth ratio equal to 1.1, the number of cells per x_1x_2-plane equal to 11800 and the number of planes in the periodic direction equal to 60. Regarding the boundary conditions, a turbulent channel flow at $\mathrm{Re}_\tau = 395$ is set at the inflow. Hereafter, this case is named *BFS-DNS* .

- **Round unheated compressible jet**

  The immersed jet exiting from a conical nozzle at $M_{\mathrm{jet}} = 0.9$ and $\mathrm{Re}_D = 1.1 \times 10^6$ based on the jet diameter D and jet exit velocity U_{jet} is considered. The resulting flow dynamics are similar to cases studied experimentally by several authors in the literature [28–32]. The computational domain, mesh and boundary conditions can be obtained from the study carried out by Shur et al. [33]. Afterwards this case was used in different investigations [14, 34]. It is considered to be a reference configuration for assessing the RANS to LES transition capabilities of different SLS and $D_{\mathrm{sgs}}(\bar{\boldsymbol{u}})$ in compressible flows. The simulation of the jet follows a two-stages approach when nozzle and jet-plume computation is performed using RANS at the first stage, while only the jet-plume region is considered at the second stage, with profiles from the first stage imposed at the nozzle exit boundary surface. These profiles of gas-dynamic and turbulence model variables were provided by M. Shur and M. Strelets from Peter the Great St. Petersburg Polytechnic University. The structured (hexahedral) Grid 3 from the papers [33] is used for

computations of the jet case. It has 160 cells in the azimuthal direction and contains $8.87M$ nodes in total.

B. Codes

Both codes employ a time integration implicit second-order scheme, doing several iteration stages per time step to achieve the desired degree of convergence. The Courant number has been kept below unity in the LES zone to ensure a proper triggering of turbulence. Both codes use the hybrid convective scheme suggested by Spalart et al. [35], switching from Symmetry-Preserving to Upwind-based depending on the flow behavior. Where the upwind dissipation vanishes in LES areas, whereas it is activated in RANS and some critical zones to guarantee system stability. particularities of each code are described hereafter.

- *OpenFOAM-v1706*

  This well-known open-source CFD code is based on an unstructured collocated finite-volume approach. The hybrid convective scheme used in this case is a blending of a second-order central difference in the LES region and a second-order upwind-biased scheme in the RANS and irrotational area. Considering broad usage of *OpenFOAM* in the CFD community, the authors have considered adding some extra details about the solvers used in the above-mentioned simulations. The BFS cases have been solved with the *PisoFoam* solver, which is recommended for transient CFD flow simulations such as LES and DDES. *SonicFoam* has been selected for the compressible flow simulations of the jet after providing the best results for transonic flows in transient simulations. Oficial versions of the solvers have been used in all simulations.

- *NOISEtte*

  The numerical algorithm realized in the research code *NOISEtte* [24] is based on quasi-1D vertex-centered EBR (Edge-Based Reconstruction) schemes [36, 37]. These schemes combine the advantages of structured and unstructured methods and provide a reasonable balance between accuracy and computational costs in scale-resolving simulation. On arbitrary unstructured meshes, the EBR schemes are theoretically of maximum second-order depending on the type of mesh elements and duals. Regarding the convective scheme, *NOISEtte* used a 4th order centered and 5th order upwind schemes in the LES and RANS areas, respectively.

IV. Results and Discusions

The results provided here have been obtained employing the *GAM* techniques shown in table 1. They have been grouped by case, which are defined in subsection III.A.

A. Zero pressure gradient flat plate

A preliminary study is carried out to evaluate the possible effect of the GAM on the shielding function, f_d, for DDES. The following computations were carried out using the *NOISEtte* research code.

Table 1 *GAM* **techniques considered in this paper. The new approach is marked with** (*).

	SLS	$D_{sgs}(\bar{\boldsymbol{u}})$
	Δ_{SLA}	SMG
(*)	Δ_{lsq}	SMG
		$S3PQR$
	$\tilde{\Delta}_{\omega}$	SMG
		σ

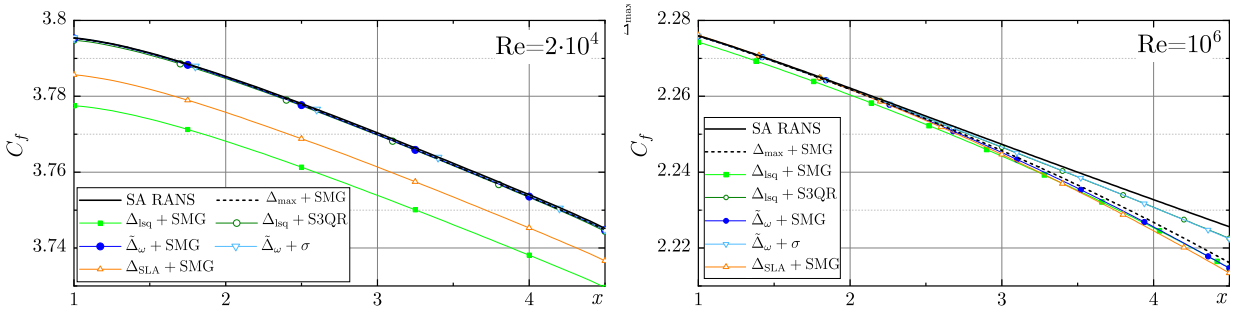

Fig. 3 **Turbulent boundary layer over the zero gradient flat plate: the friction coefficient distributions, C_f, over the wall for** $\mathrm{Re} = 2 \cdot 10^4$ **(left) and** $\mathrm{Re} = 10^6$ **(right) using different GAM approaches.**

Figure 3 shows the C_f distributions in the stream-wise direction calculated using all the GAM approaches considered in the present paper. The SA RANS and original DDES formulation (with $\Delta_{max} + SMG$) results in the figure are provided from Spalart et al. [1] as reference. It can be seen from the graphs that using either Δ_{SLA} or Δ_{lsq} with the SMG model leads to slight underestimation of the C_f for both Reynolds numbers tested (note the y-axis scale is different in each case). However, it is noted that in both cases the gradient is similar to the standard $\Delta_{max} + SMG$ solution and does not exceed 1% error for $\mathrm{Re} = 2 \cdot 10^4$ (even lower for $\mathrm{Re} = 10^6$). Regarding the other models tested (variants of $\tilde{\Delta}_{\omega}$ and S3QR), figure 3 indicates an improved correlation with the reference RANS solution. The modest improvement is anticipated, due to th re-calibration of the empirical constant C_{d1} (used for calculating the f_d function) presented by Mockett et al. [27], whereas the original value of this constant has been retained in the other models. In conclusion, the data presented above indicates that the different techniques considered in the paper do not lead to any noticeable drawbacks in the shielding function.

B. BFS: Vogel & Eaton (*BFS-VE*)

The triggering of oscillations in the free shear layer appears to be linked to an improved resolution of the flow dynamics in the LES region. In this regard, the influence of different *GAM* strategies into such oscillations downstream the step-edge are studied by means of rms(u') (figure 4). While there is no experimental or high-quality numerical data providing the correct level of oscillations in such area, it can be observed using both codes how the new SLS, Δ_{lsq}, triggers slightly higher fluctuations than the standard strategies for mitigating the *GA*. Especially at the free shear layer

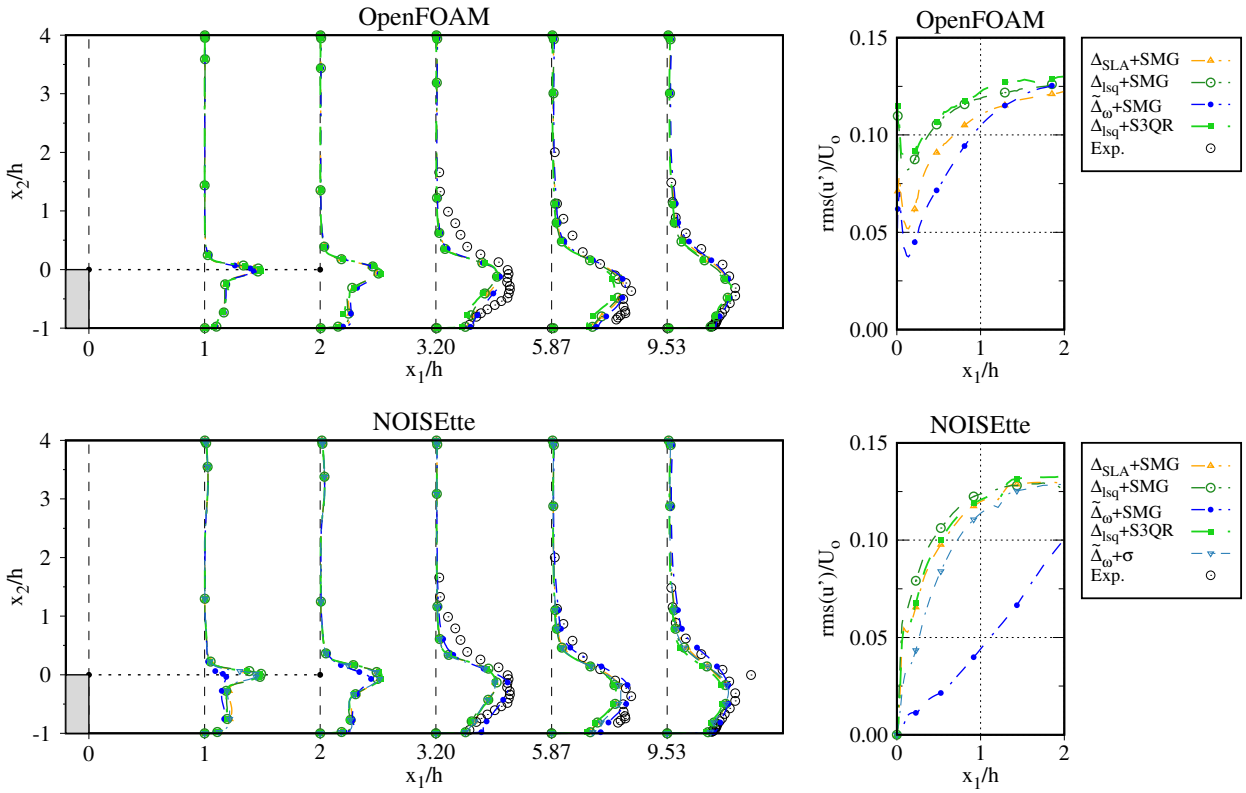

Fig. 4 *BFS-VE* **: Backward Facing Step from Vogel and Eaton [20]** ($\mathrm{Re}_\tau = 2500$, $ER = 5/4$)**. Different combinations of Subgrid Length Scales and Differential Operators, plotted for both codes: (top)** *OpenFOAM* **and (bottom)** *NOISEtte* **. (left) wall normal profiles of the streamwise component of fluctuating velocity,** $\mathrm{rms}(u')$**, and (right) evolution of the same quantity along the horizontal line,** $x_2 = 0$**, directly downstream of the step corner.**

area, close to the step edge. The fact that $\tilde{\Delta}_\omega + SMG$ is clearly not aligned with the rest of SLS is caused by the delay in the RANS to LES transition, leading to energetic oscillations downstream of the flow. The differences observed in figure 4 between the SLS strategies at the free shear layer area can be explained by drawing a comparison between earlier results for homogeneous flows, shown in figure 1 and the Δ distribution downstream the step-edge in figure 5. As expected, $\Delta_{\max}$ returns the highest Δ values, translating to higher dissipation in the shear layer, so contributing to an excessive delay of the flow instabilities in such regions. A probe of that are the studies carried out by Shur et al. [14] and Guseva et al. [15]. An important reduction of Δ is shown in figure 5 when using $\tilde{\Delta}_\omega$, as a 2D flow behaviour in the $x_1 x_2$ plane downstream of the step-edge is detected (*GA* region), ignoring Δx_3 and getting closer to the diagonal value in this plane; $\tilde{\Delta}_{\omega-2D} = \sqrt{(\Delta x_1^2 + \Delta x_2^2)/3}$. It is worth noting here that $\tilde{\Delta}_\omega$ will never provide values lower than the lowest 2D diagonal of the cell,

$$\tilde{\Delta}_{\omega\min} = \min_{i!=j} \left(\sqrt{(\Delta x_i^2 + \Delta x_j^2)/3} \right). \tag{12}$$

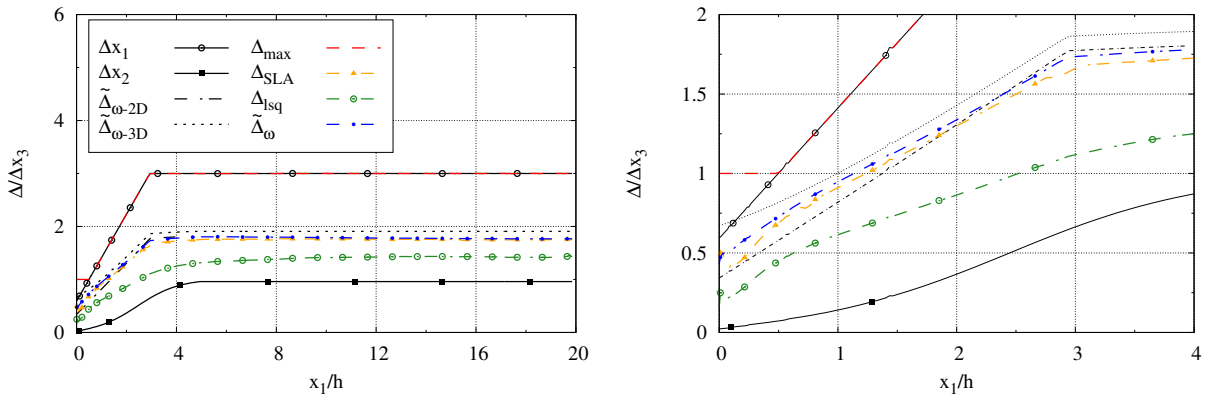

Fig. 5 *BFS-VE* **: Backward Facing Step from Vogel and Eaton [20]** ($\mathrm{Re}_\tau = 2500$**,** $ER = 5/4$**). Variation of grid refinement and cell aspect ratios (in direction** x_1 **and** x_2**) compared time-averaged values of the different Subgrid Length Scale formulations tested, as defined in section II. Values are plotted for (left) the full domain downstream of the step corner and (right) a zoom of the region near the step. Resulst from** *OpenFOAM* **.**

In this case, $\tilde{\Delta}_\omega$ and $\tilde{\Delta}_{\omega-2D}$ do not completely collapse, due to the undesirable numerical oscillations present at the very beginning of the step-edge (rms values in figure 5, left, at $x_1/h = 0$ are not 0). Therefore, these oscillations lead to Δ values which are representative of $3D$ structures, i.e. $\tilde{\Delta}_{\omega-3D} = \sqrt{(\Delta x_1^2 + \Delta x_2^2 + \Delta x_3^2)/3}$ rather than 2D, $\tilde{\Delta}_{\omega-2D}$ (figure 5), affecting also the Δ_{SLA} natural behaviour, as it is not deactivated close to the step-edge. The reason why these fluctuations are catalogued as undesirable is because they cannot have a physical origin, as these would be easily dumped for the high dissipation present in the RANS area. The proper physical oscillations would have a progressive rise through the shear layer, similar to the one shown by the DNS data (figure 7). Considering the impact of these unwanted numerical oscillations in the overall simulation, a special test has been carried out in the next case in order to understand their possible origin. The authors think that they could be induced by the high aspect ratios at the step-edge ($\Delta x/\Delta y \sim 32$), which is supported by the fact that these oscillations have only been observed in the results obtained with *OpenFOAM* (figure 4).

In contrast to $\tilde{\Delta}_\omega$, for which the minimum value is proportional to the Euclidean norm as described in Eq. 12, the Δ_{lsq} formulation permits to take values of Δx_2 directly, i.e. significantly smaller than the Euclidean norm in the vicinity of the wall. This interesting property was noted previously in section II and in figure 1 for "Simple Shear" dynamics. This feature is thus highly relevant to the BFS, and many other configurations exhibiting similar separation and subsequent development of instabilties in the shear layer. The small Δ values lead to a strong reduction of the eddy-viscosity, generally unlocking the *KH* instabilities and improving the quality of the simulation in the LES region. However, while we can observe in figure 5 how Δ_{lsq} follows a similar trend as Δx_2 distribution, there is a clear offset, mainly produced by the initial oscillations at the step-edge. It explains why the transition from "Simple Shear" to "Pure Rotation" cannot be completely appreciated in figure 5 (both terms are defined in figure 1). It is important noting here that Δ_{lsq} still presents the lowest values of Δ, which explains the good behaviour of the oscillations observed in figure 4.

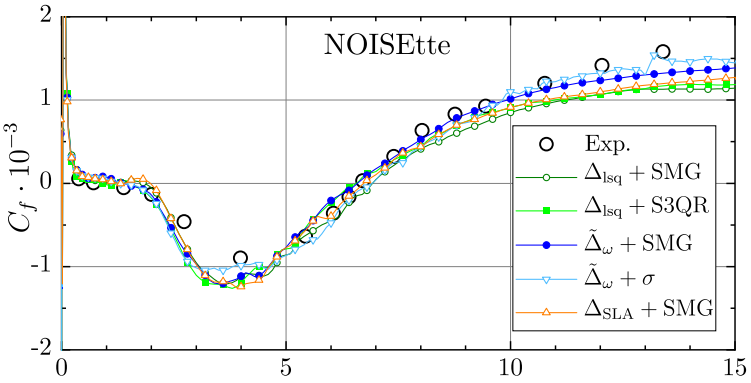

Fig. 6 Skin friction coefficient C_f distribution over the lower wall considering various SLS in combination with different $D_{\mathrm{sgs}}(\bar{\boldsymbol{u}})$. Experimental data, $Exp.$, has been obtained from Vogel and Eaton [20].

Regarding the results obtained with other differential operators, we can note that combining $\tilde{\Delta}_\omega$ with a 2D-sensitive formulation, such as σ, results in a significant improvement in the free shear layer area (figure 4). This is in good agreement with the observations carried out by previous authors [12, 13]. This is not the case for $\Delta_{\mathrm{lsq}} + S3QR$, which presents almost no difference in comparison with $\Delta_{\mathrm{lsq}} + SMG$. Figure 4 also demonstrates that very similar trends are observed in both codes, *OpenFOAM* and *NOISEtte*, which is clearly a good indication of the reliability and code independence of the new approach.

Figure 6 presents the skin friction coefficient $C_f = \tau_w / \left(0.5 \rho_0 U_{max}^2\right)$ (here U_{max} is the centerline velocity at the channel inflow) distributions over the lower wall downstream the step. It is seen that the results using all the considered approaches correspond well to each other and to the experimental values. The flow aerodynamics including reattachment point location is captured precisely. A slight deviation can be distinguished only at the region downstream $x/h \geq 8$ where the flow is simulated in the WMLES regime where the DDES approach does not provide appropriate accuracy.

While the *BFS-VE* case is an important reference for hybrid methods, the lack of detailed reference data in the free shear layer region reduces the scope for a more detailed analysis of model performance. For this reason, a comparison with DNS data has been performed in the next section, using another *BFS* configuration [21]. In particular, it enables a detailed examination of the intriguing oscillations which appear just after the step-edge in the *OpenFOAM* . They are anticipated to be due to the high cell aspect ratio in this area, $\Delta x_1 / \Delta x_2 \sim 32$, but their relation is not clear. As such, a set of meshes with different aspect ratios and refinements downstream the step-edge are tested in the *BFS-DNS* case.

C. Instabilities' growth at the shear layer (*BFS-DNS*)

As identified in the previous section, the motivations for considering this case; 1) to investigate performance of the new approach in free shear layer region and 2) to assess their sensitivity to high aspect ratio cells in this region. For this purpose, three meshes with slightly different x_1 refinements in the shear layer area have been considered (keeping constant Δx_2), with the following cell aspect ratio at the step edge, $\Delta x_1 / \Delta x_2 = 32$, 16 and 8. The performance of the new

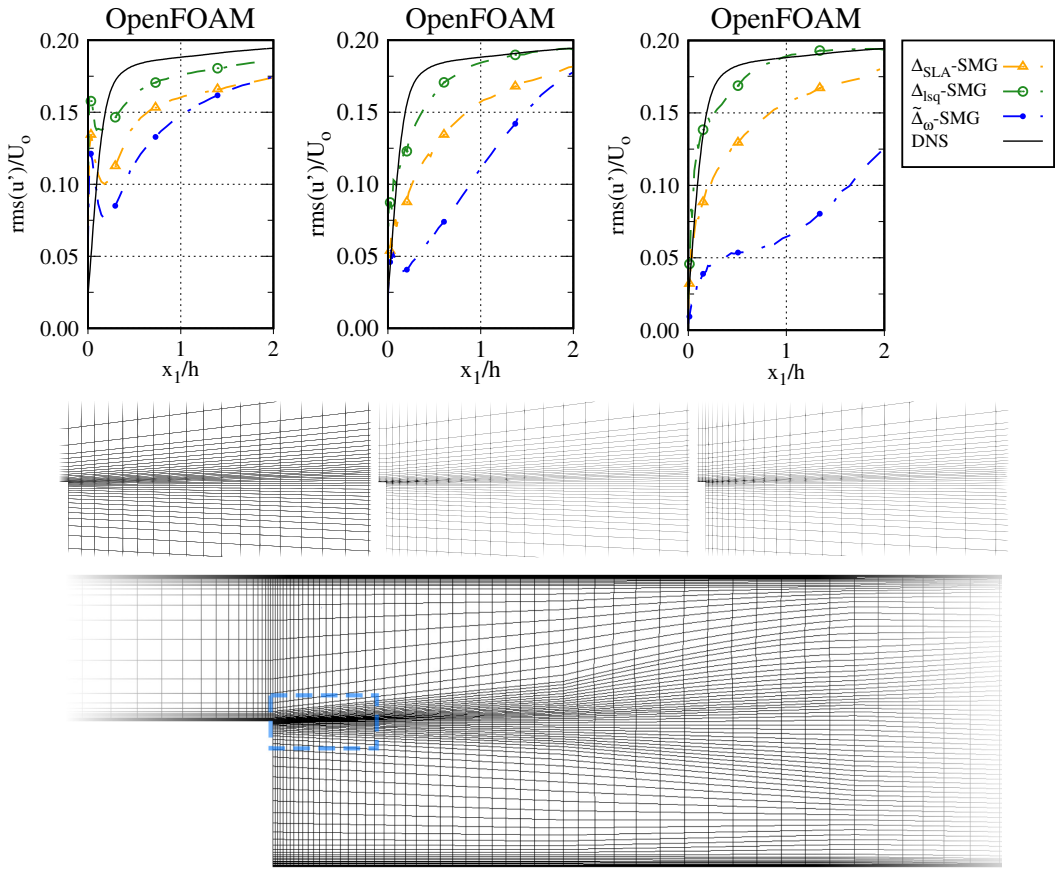

Fig. 7 *BFS-DNS* **: Backward Facing Step from Pont-Vílchez et al. [21]** ($\mathrm{Re}_\tau = 395$, $ER = 2.0$)**. Impact of reducing the cell aspect ratio in the streamwise direction on prediction of fluctuating velocity,** $\mathrm{rms}(u')$**, downstream of the step corner (left to right:** $\Delta x_1/\Delta x_2 = 32, 16, 8$**). A detailed zoom view of the mesh used for each simulation is provided just below** $\mathrm{rms}(u')$**, together with a zoom out view. Results obtained with OpenFOAM.**

approaches in such meshes is presented in figure 7, demonstrating the influence of the the cell aspect ratio in the rms(u') distribution. In addition to observing that stronger fluctuations are triggered by Δ_{lsq} compared to the other candidates, we can also appreciate the good alignment with the DNS dataset. This supports the hypothesis that Δ_{lsq} contributes to an improved definition of the *KH*-instabilities in the shear layer region. Furthermore, it seems that the observed oscillations just after the step-edge are strongly mitigated when the cell aspect ratio in this region is reduced. Other interesting interpretations can be made from figure 7, such as the strong mesh resilience presented by Δ_{lsq} and Δ_{SLA} in comparison to $\tilde{\Delta}_{\omega}$. The poor performance of $\tilde{\Delta}_{\omega}$ observed in figure 7 (left) is attributed to the cell's stream-wise size (at $x_1/h \sim 1$) and the strong dependence of $\tilde{\Delta}_{\omega}$ on this value. This is not true for other definitions of SLS; namely, Δ_{SLA} is significantly reduced for (quasi-)2D flows (like in this case) whereas Δ_{lsq} has a very small dependence of Δx_1 at the beginning of the shear layer where the flow resembles the idealized simple shear configuration (see figure 1). Of course, at more downstream locations, shear-layer instabilities start to develop leading to more complex flow configurations where Δx_1 will play a relevant role in the calculation of Δ_{lsq}. This process can be viewed as a natural transition from simple-shear-like configuration towards a more pure-rotation-like (*KH* vortices), where both Δ_{lsq} length-scale and $\tilde{\Delta}_{\omega}$ have a similar behavior (see figure 1). Finally, it also seems that while there appears at first glance to be some 'benefit' of these unphysical oscillations in the development of turbulence downstream of the step, this is likely to be fortuitous, since the tests for $AR = 32$ never entirely recover the DNS levels of rms(u'). The subsequent analysis considers only the mesh with $\Delta x_1/\Delta x_2 = 16$. The rms distributions along the stream-wise direction are presented in figure 8. In addition to a significant improvement of $\Delta_{\text{lsq}} + SMG$ in comparison to $\tilde{\Delta}_{\omega} + SMG$ and $\Delta_{\text{SLA}} + SMG$ at the shear layer, all SLS behave similarly downstream of the step-edge ($x_1 > 2$) for both codes. A general misalignment is seen at $x_1 = 8$, which is attributed to the lack of mesh resolution in this region. The positive effect of using a 2D sensitive differential operators, such as σ, in combination with $\tilde{\Delta}_{\omega}$ is demonstrated once again in the free shear layer area (figure 8, right). In a similar way to in the previous case, there was almost no sensitivity of Δ_{lsq} to the $D_{\text{sgs}}(\bar{\boldsymbol{u}})$ used, as as observed in the *BFS-VE* case, similar results are obtained with both codes, *OpenFOAM* and *NOISEtte*.

The same conclusions can be obtained in figure 9 with the view map (plane-x_1x_3) of the Q_{G} isosurfaces in the shear layer area, showing the turbulence generated in such region, just after the step edge $x_2 = 0$. These images clearly show how the level of turbulence is significantly higher in $\Delta_{\text{lsq}} + (SMG, S3QR)$ than in the other strategies, which is in good agreement with the other observations commented before.

Finally, a study of the instabilities' growth at the shear layer is provided, where we can observe how it behaves with different *GAM*. The same methodology described in Pont-Vílchez et al. [21] is used. A schematic view of the instabilities's growth is shown in figure 10. First, a set of 2-point correlations of u_2' along the stream-wise direction downstream of the step-edge (figure 11) has been used for calculating the size of the instabilities in the stream-wise direction, $\Delta\delta_1$. Unfortunately, the RANS flow coming from the inflow, makes this technique unusable for estimating $\Delta\delta_2$,

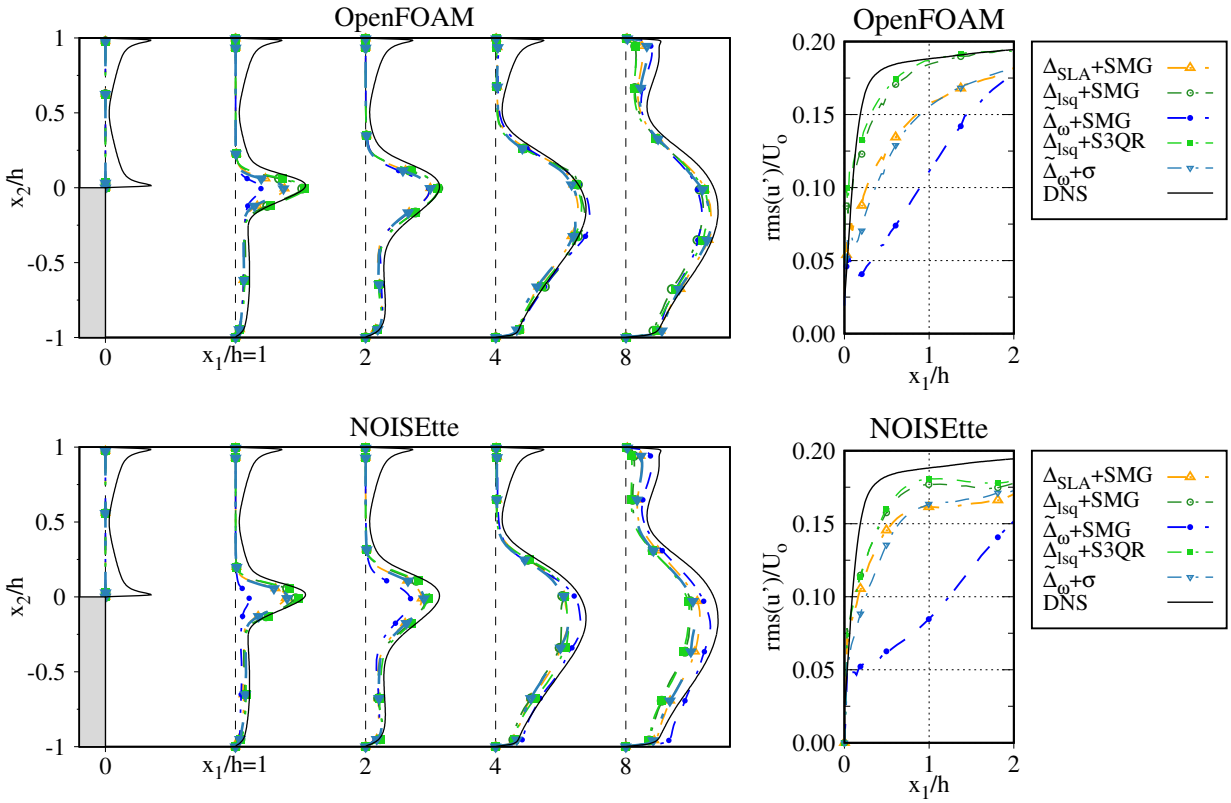

Fig. 8 *BFS-DNS* **: Backward Facing Step from Pont-Vílchez et al. [21]** (Re_τ = 395, ER = 2.0)**. Different combinations of Subgrid Length Scales and Differential Operators, plotted for both codes: (top)** *OpenFOAM* **and (bottom)** *NOISEtte* **. (left) wall normal profiles of the streamwise component of fluctuating velocity,** rms(u')**, and (right) evolution of the same quantity along the horizontal line,** x_2 = 0**, directly downstream of the step corner.**

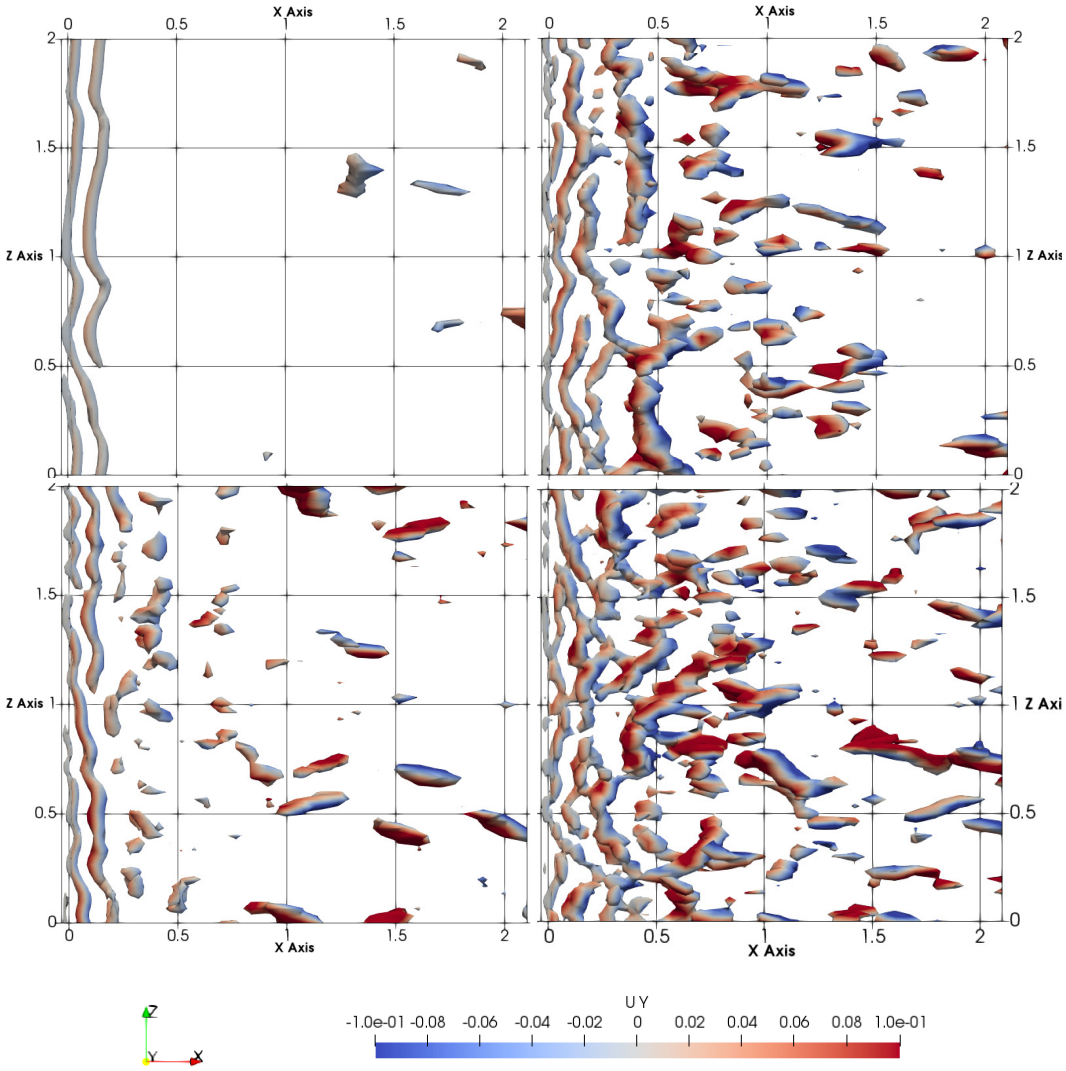

Fig. 9 View map (plane-$x_1 z_3$) of the Q_{G} isosurfaces, $Q_{\mathrm{G}}(H/U_b)^2 = 10$, for the following *GAM* strategies: $\tilde{\Delta}_{\omega} - SMG$ (top-left), $\Delta_{\mathrm{lsq}} - SMG$ (top-right), $\Delta_{\mathrm{SLA}} - SMG$ (bottom-left), $\Delta_{\mathrm{lsq}} - S3QR$ (bottom-right). The dimensionless velocity field in x_2 direction is plotted in the isosurfaces.

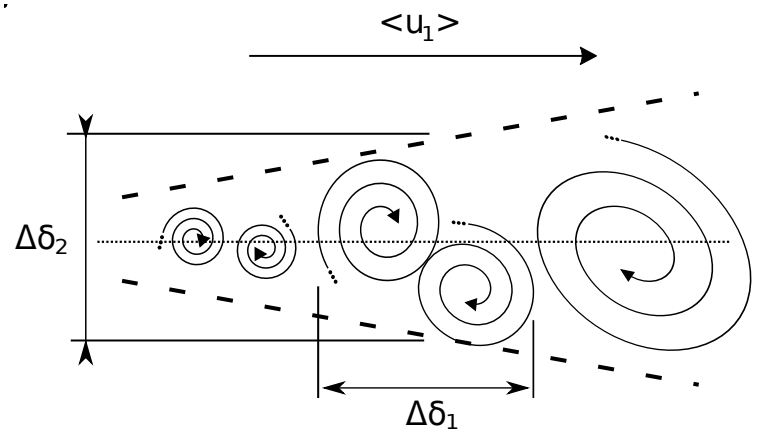

Fig. 10 Schematic view of the Kelvin-Helmholtz vortices in a shear layer, where $\Delta\delta_1$ and $\Delta\delta_2$ represent a estimation of the vortex size in the stream-wise and normal direction, respectively.

so another approach has been used [21, 38],

$$\Delta\delta_2 = \Delta U_1 / (\partial \langle u_1 \rangle / \partial x_2)_{\max}. \tag{13}$$

In figure 8 we can see how the rms profiles are highly influenced by the *SLS* along the shear layer. However, this is not so significant in the $\Delta\delta_1$ distribution (figure 11, top). The best alignment is shown by Δ_{lsq} and Δ_{SLA} at $x_1 \in [0, 0.8h]$. It can also be observed how this initial correlation with DNS data is considerably reduced downstream, exhibiting a shallower slope in comparison to $\tilde{\Delta}_\omega$ and the DNS. The coarsening of the mesh in such region can explain this deterioration. While the results for $\tilde{\Delta}_\omega$ appear to indicate a slope gradient in closer accordance to the reference data, this is likely associated to the overestimation observed in $0.4 \leq x_1 \leq 0.7$.

Regarding $\Delta\delta_2$, it seems to be quite sensitive to the SLS (figure 11, bottom). This was an expected behaviour as the terms used for estimating $\Delta\delta_2$ (Eq.13), indirectly depends on other terms which are highly influenced by SLS, such as rms(u'). Hence, figure 11 (bottom) clearly demonstrates once again how diffusion introduced by Δ_{SLA} and $\tilde{\Delta}_\omega$ is too high to ensure the correct development of the *KH* instabilties along the shear layer.

Figure 12 presents the skin friction coefficient $C_f = \tau_w / \left(0.5\rho_0 U_{\max}^2\right)$ distributions over both the upper and lower walls downstream the step. As for the BFS-VE case, the results using all the considered approaches correspond well to each other. It could be concluded that shielding property of the DDES approach with the new proposed techniques remains the same as the original DDES model or the DDES with shear-layer adapted length scale [14]. The perceptible difference in the upper-wall between the DDES results and the reference DNS data can be attributed to the insufficiency of the DDES approach for dealing with such configurations where the shear layer's resolved turbulence interfere with the WMLES area at the upper wall.

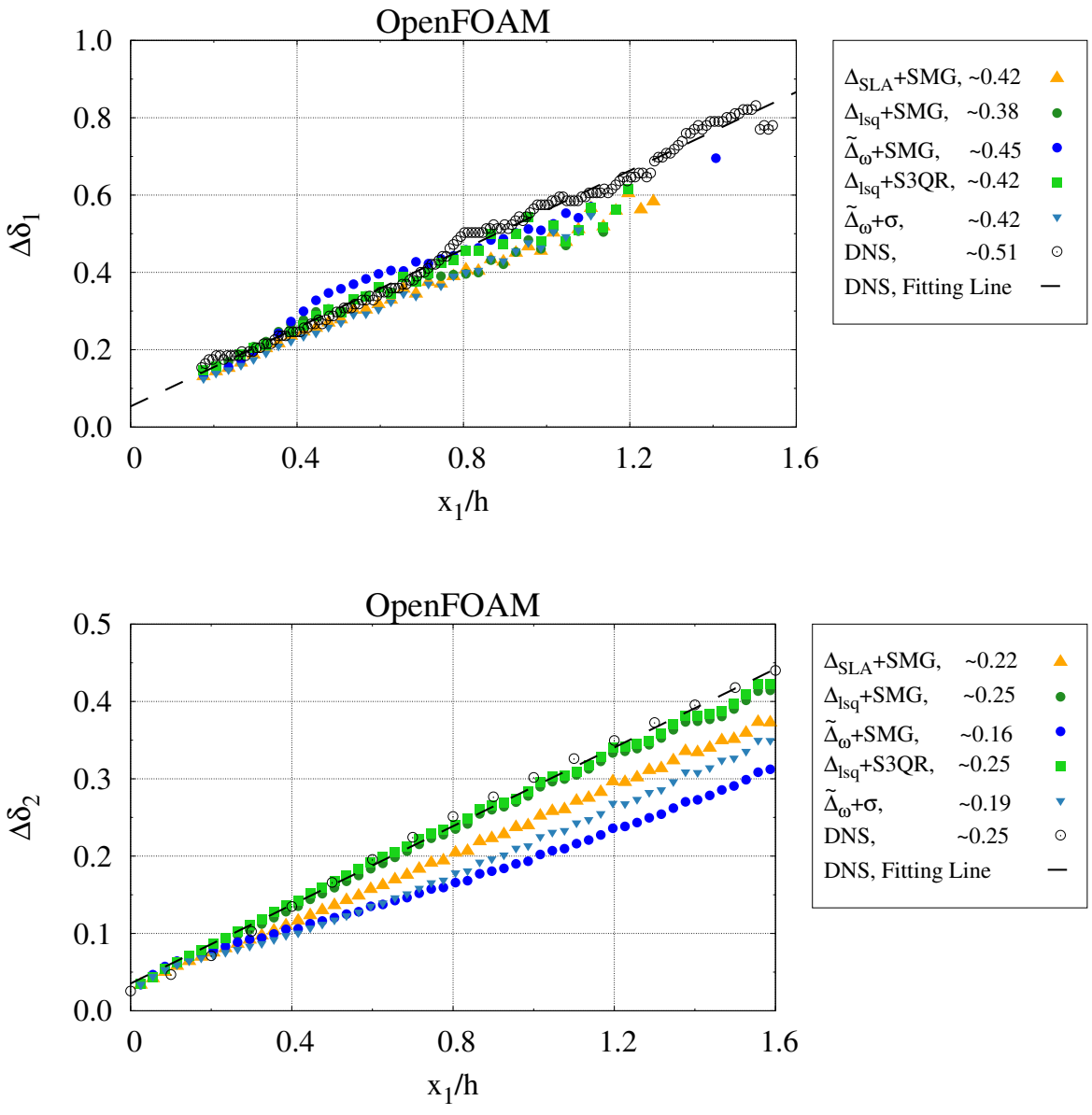

Fig. 11 *BFS-DNS* **: Backward Facing Step from Pont-Vílchez et al. [21]** (Re_τ = 395, ER = 2.0)**. Impact of Subgrid Length Scale choice** *KH* **rate of growth in the (top) stream-wise and (bottom) normal directions downstream of the step-edge;** $\Delta\delta_1$ **and** $\Delta\delta_2$ **respectively. In each case, the gradient of linear regression is given in the legend.**

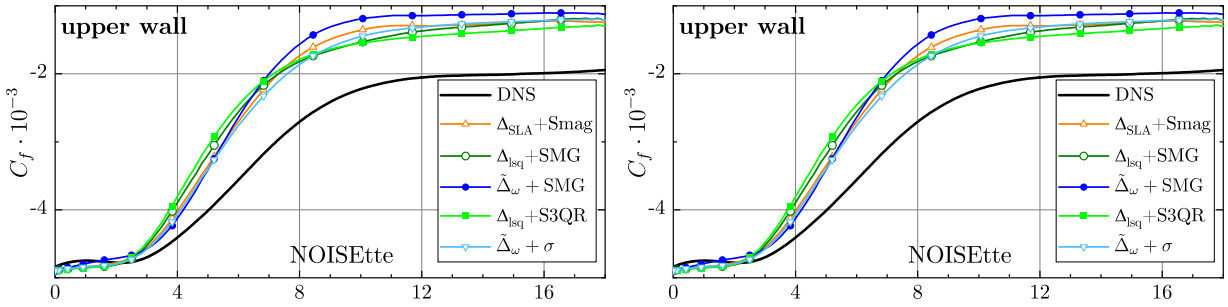

Fig. 12 Skin friction coefficient C_f distribution over the upper (left) and lower (right) wall considering various SLS in combination with different $D_{\text{sgs}}(\bar{\boldsymbol{u}})$. A DNS [21] has been used as reference data.

D. Round unheated compressible jet

The jet plume region characteristics obtained using different approaches realized in both codes (*NOISEtte* and *OpenFOAM*) are presented on the figures 13-17. In terms of the correspondence with the reference data, the first observation is that all approaches evaluated in this paper capture the jet dynamics reasonably well, with the exception of one model. The limited capability for *GA* mitigation of the $\tilde{\Delta}_\omega$ length scale in the jet case is expected and was already reported in previous studies [7, 14, 22].

Figures 13 and 14 present a comparison of the averaged stream-wise velocity and its rms distributions, correspondingly, over the jet centerline. All the approaches (except $\tilde{\Delta}_\omega + SMG$) allow to predict the length of the jet core region more or less correctly. The results obtained using the *NOISEtte* research code are notably more consistent than the *OpenFOAM* ones. This behaviour could be due to the numerical scheme employed for convective fluxes and its dissipation properties. *NOISEtte* uses the higher accuracy EBR scheme which exploits extended stencils to achieve higher resolution which results in less dissipation from the numerical scheme. Both less dissipation and higher accuracy (in terms of absolute value of the numerical error) lead to an earlier RANS-to-LES transition in the shear layer, avoiding sudden exposure-like wakes or numerical instabilities. This observation is supported by figure 14, where the rms levels of stream-wise velocity in the results obtained with *OpenFOAM* start to grow permanently, in the region $2x/D$ till $3.5x/D$ and are noticeably overestimated by the region $5 < x/D < 10$, in contrast to the corresponding distributions obtained using the *NOISEtte*. A faster RANS-to-LES transition also facilitates more "physical" evolution of the shear layer downstream which is developed more smoothly. After reducing a maximum between $10 < x/D < 12$, the centerline distributions of rms(u') obtained by all the considered *GA* mitigation approaches and both codes are close to each other and to the experimental values.

A more in-depth evaluation of performance is now considered by analyzing the distributions of various characteristics along the lip line downstream of the nozzle edge; presented in the figures 15-17. The averaged subgrid length scale normalized by its maximum, Δ_{max}, local value and turbulent to molecular viscosity ratio are shown on the figures 15 and 16, correspondingly. By analyzing these plots the following features can be revealed. First of all, none of the considered

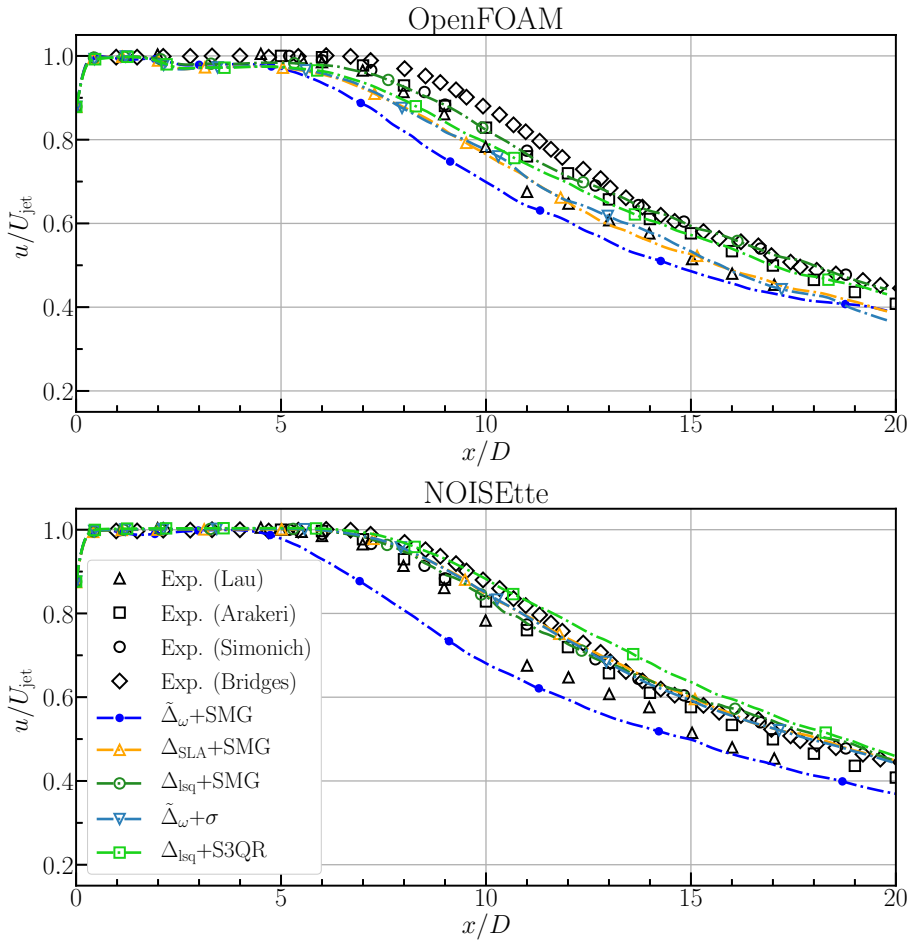

Fig. 13 Average of the stream-wise velocity over the jet center line starting from the jet nozzle exit.

subgrid scales ($\tilde{\Delta}_\omega$, Δ_{SLA} and Δ_{lsq}) does reach Δ_{max} value. It is observed in the early shear layer region that is highly desirable to provide the faster RANS-to-LES transition. As for the areas far downstream the nozzle exit, Δ_{sgs} values are lower than Δ_{max} because of the anisotropy of the mesh used in the simulations along the lip line. It does not lead to any drawbacks: the Δ_{sgs} distributions behave like $O(\Delta_{\text{max}})$ remaining much higher than Δ_{min}. Note that the realization of static scales Δ_{min} and Δ_{max} slightly differs in the codes. The *OpenFOAM* inherits the classical realization: the projection of the cell to the Cartesian axes. As for the *NOISEtte* , vertex-centered Δ_{min} and Δ_{max} values are calculated as the minimum and maximum height of the hexahedrons incident to the node, correspondingly. So these values (and another Δ_{sgs} relative to Δ_{max}) differ from each other, especially in the areas where gridlines are not parallel to the axes.

Another obvious property is that the Δ_{lsq} values and, accordingly, turbulent viscosity levels are significantly lower than those provided by $\tilde{\Delta}_\omega$ and Δ_{SLA} length scales. In the very early shear layer region (see the right plots of figure 15), at $x/D \lesssim 0.1$, the Δ_{SLA} length scale drops to very low values with strong growth till $x/D \approx 0.3$ (due to impact of $F_{\text{KH}}(\langle\text{VTM}\rangle)$ function). The Δ_{lsq} is proportional to Δ_{min} before $x/D = 0.2 - 0.3$. After $x/D = 0.3$ both length scales (Δ_{SLA} and Δ_{lsq}) have the same increasing trend up to $x/D \approx 0.9$. In the developed shear layers regions,

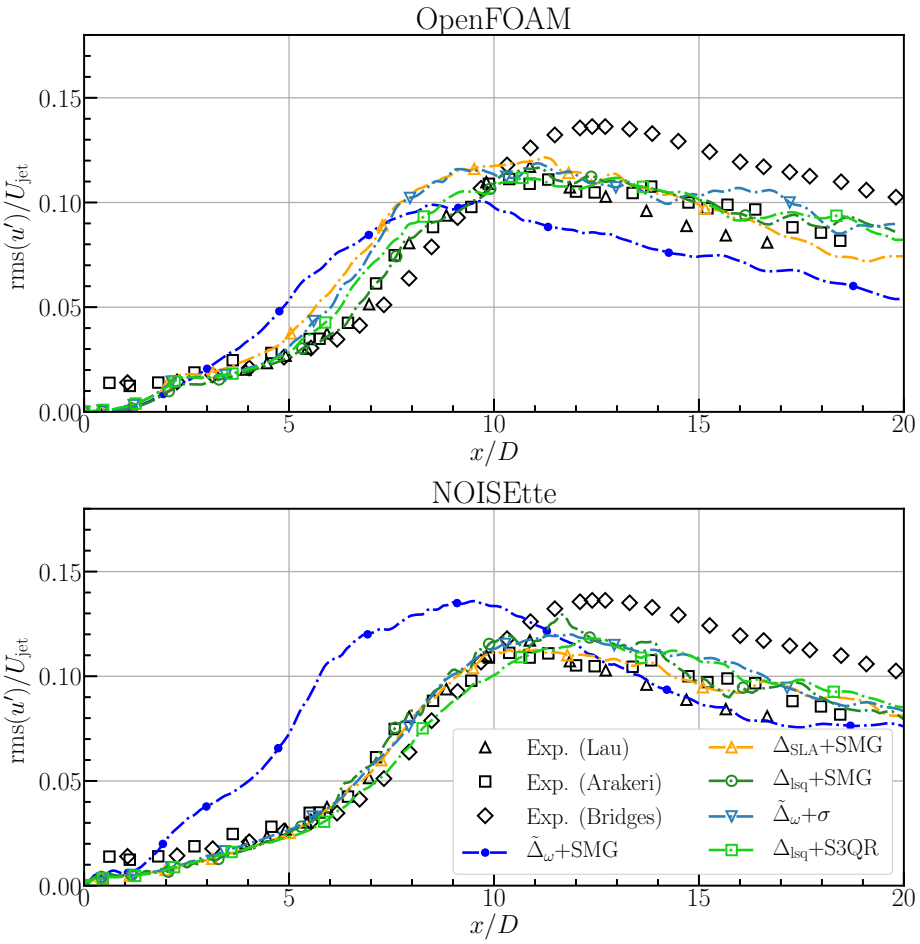

Fig. 14 Average of the stream-wise velocity root-mean square over the jet center line starting from the jet nozzle exit.

with resolved 3D turbulence, the Δ distributions behave like $O(\Delta_{\max})$ with slight deviation in the approximate region $0.4\Delta_{\max} < \Delta < 0.7\Delta_{\max}$. The turbulent viscosity levels presented on the figure 16 mostly follow the corresponding subgrid length scale values' trends. The distributions of stream-wise velocity rms values are presented on the figure 17. Overall, all the considered approaches result in a good correlation with the reference data and with each other. It is being observed for both codes, *NOISEtte* and *OpenFOAM*, too. The only noticeable discrepancy can be revealed in the early shear layer region at $0 < x/D < 2$: the peak values of rms(u') from the *OpenFOAM* simulations are higher than the *NOISEtte* ones. It can be attributed to the behaviour of the numerical scheme for convective fluxes (as already mentioned above in this subsection): low dissipativity and higher accuracy of the numerical scheme facilitate earlier RANS-to-LES transition. This is why the values of turbulent viscosity from the simulations carried out by *NOISEtte* are higher than *OpenFOAM* ones (see the results using alternative SGS model on the figure 16): shear layer evolution becomes smoother, decreasing the observed amount of unphysical oscillations.

This slight delay results in a notably more intense "numerical" transition downstream, that is manifested in higher

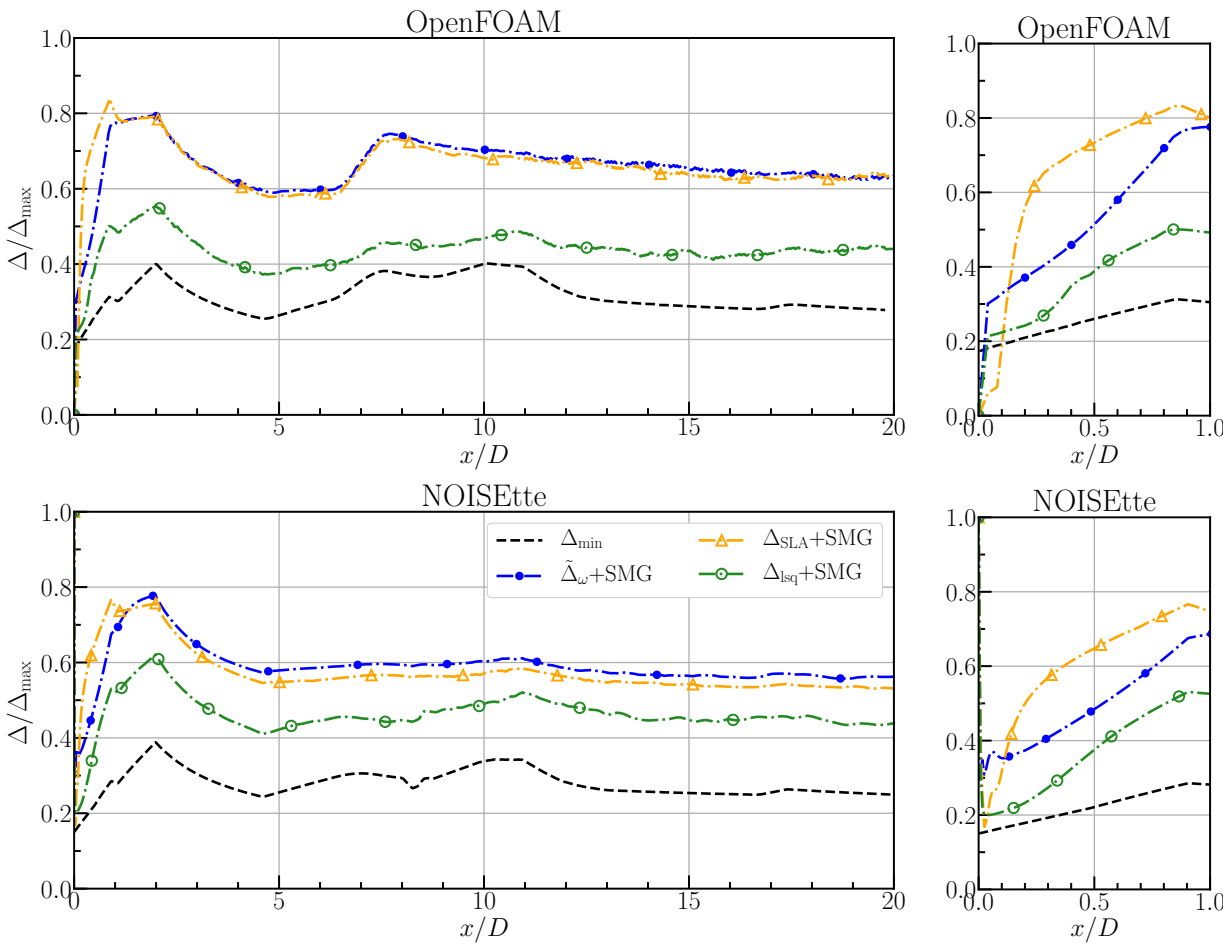

Fig. 15 Average of the subgrid length scales over the lip line starting from the jet nozzle exit (left) and its zoom view near the edge (right).

levels velocity rms distributions in this part of the shear layer. It is seen from the figure 17 (right) that Δ_{SLA} provides faster development of the separated flow apparently due to the lower levels of turbulent viscosity. As also pointed out in the previous subsections (IV.B and IV.C) two peaks of stream-wise velocity rms are observed in the early shear layer region (see right subfigures of figure 17): the first lays at $x/D \approx 0.05$ in the *NOISEtte* distributions and at $x/D \approx 0.15$ in the *OpenFOAM* ones; the second – in the region $0.3 < x/D < 0.7$, depending on the method and the code used. The first peak, driven by RANS-to-LES "numerical" transition, has an unphysical nature, likely related to the mesh anisotropy in this region, while the second is attributed to the resolved turbulence in the shear layer. There are three peaks in the rms(u') distributions obtained using *OpenFOAM* when σ or $S3QR$ model is used instead of SMG (see right top plot of the figure 17). This fact can be explained by unphysical oscillations appearing in this region due to slightly delayed RANS-to-LES transition with mesh underesolution to provide it correctly when alternative LES models are applied.

The usage of alternative LES subgrid model, σ in combination with $\tilde{\Delta}_\omega$ and $S3QR$ in combination with Δ_{lsq}, perceptibly addresses the *GA* problem by ensuring much lower dissipation in the very early shear layer regions. It is

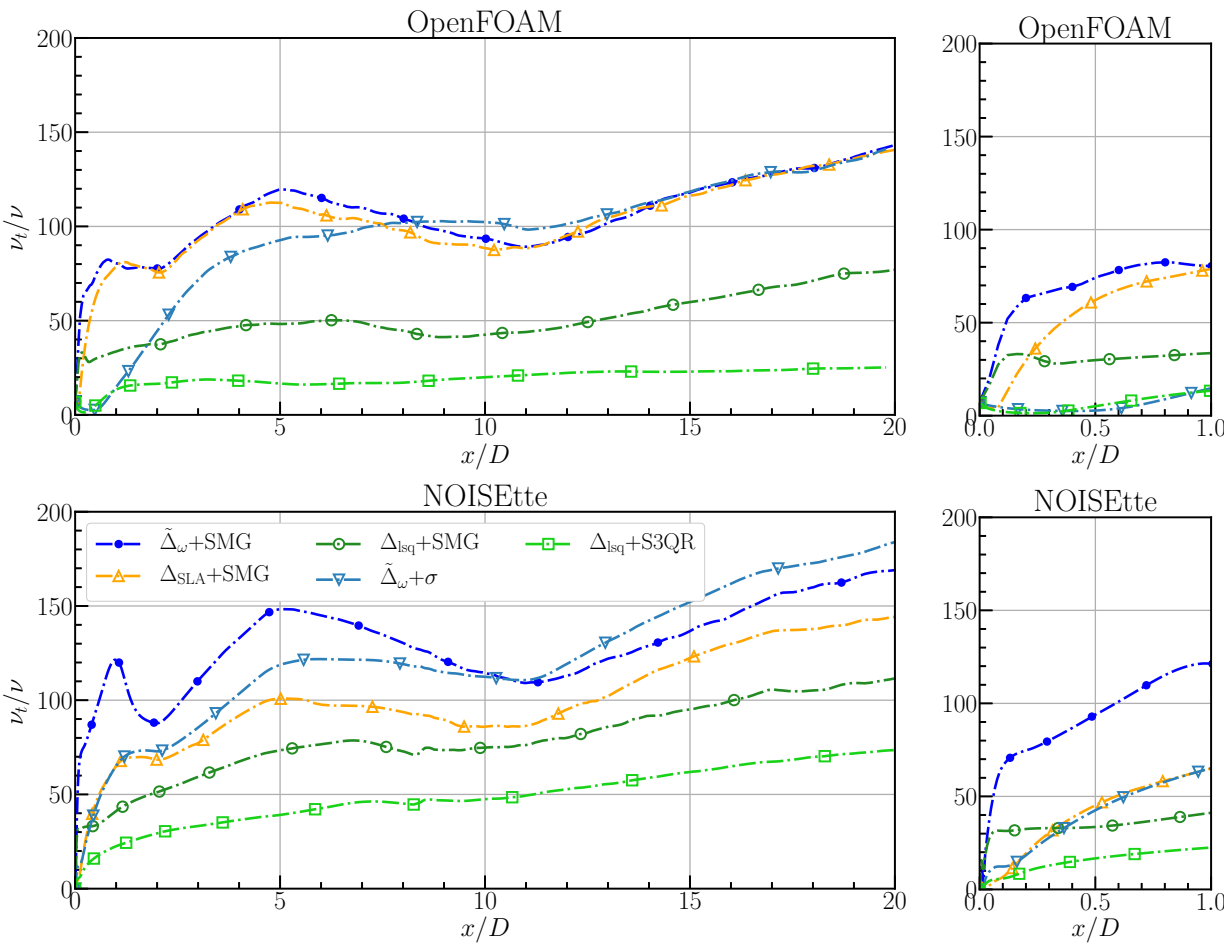

Fig. 16 Average of the turbulent to molecular viscosity ratio over the lip line starting from the jet nozzle exit (left) and its zoom view near the edge (right).

seen from figures 13, 14 and 17 that the results obtained using $\tilde{\Delta}_\omega + \sigma$ and Δ_{lsq}+$S3QR$ are in close agreement with those provided by Δ_{SLA} or Δ_{lsq} +SMG both in the jet core region ($x/D \approx 7-8$) and downstream it. It happens in spite of the fact that turbulence viscosity distributions vary from each other quite strongly (see figure 16). Whiere the σ model increases turbulent viscosity, in comparison to the results using SMG, $S3PQR$ model yields reduced levels (see figure 16). In general, the incorporation of an alternative LES model enhances the simulation of the jet and does not lead to any crucial drawbacks.

V. Conclusions

The main aim of this work was to address, or at least partly mitigate, the Grey Area issue present in DDES models by means of techniques initially developed for LES turbulence models. In both applications there is an inherent need to reduce ν_{sgs} in critical regions, where flow does not strictly behave in a fully turbulent manner. For this reason, we decided to compare some recently developed Grea Area Mitigation techniques, such as $\Delta_{\text{SLA}} + SMG$ and $\tilde{\Delta}_\omega + \sigma$, with

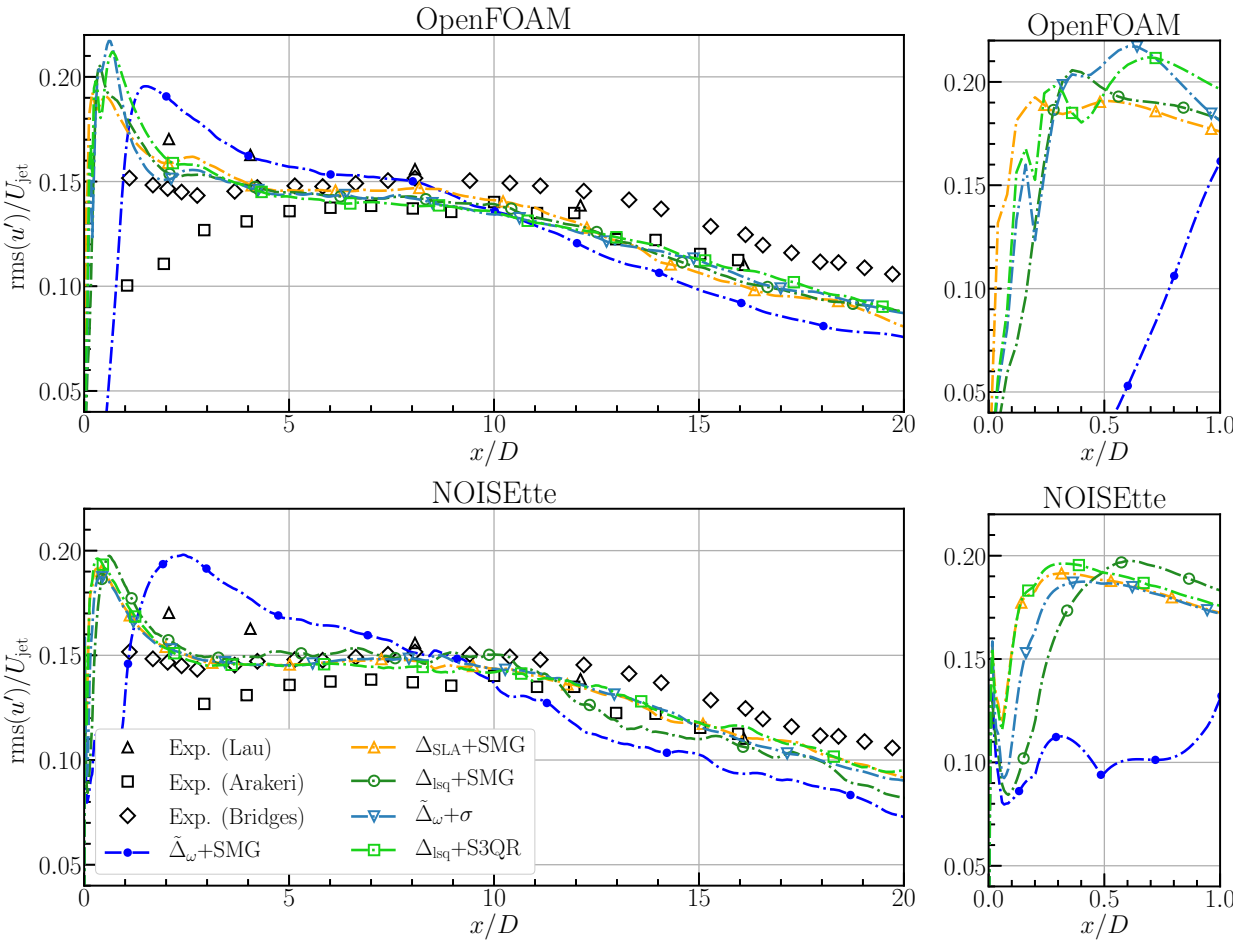

Fig. 17 Average of root mean square of the stream-wise velocity over the lip line starting from the jet nozzle exit (left) and its zoom view near the edge (right).

two new approaches initially designed for LES models (Δ_{lsq} and $S3QR$), in order to assess their ability to move from RANS to LES in areas where the flow presents a complex behaviour such as free shear layers.

The new approaches have been demonstrated to behave in a similar, and in some cases superior, manner to those techniques previously proposed to address those issues, such as $\Delta_{\text{SLA}} + SMG$ and $\tilde{\Delta}_\omega + \sigma$. This conclusion has been supported by applying the new approach to four different cases (considering incompressible and compressible flows), each computed with two different codes. As well as demonstrating improved performance, the new approaches are grounded in well-established physical LES modelling assumptions, whereas the standard GAM techniques incorporate a certain degree of tuning and blending which renders the model more empirical.

It is also worth mentioning that the beneficial influence of Δ_{lsq} is considerably more impactful than that obtained when using a differential operator sensitised to 2D flows, such as $S3QR$; the effect of these models is only noticed when the SLS is too difussive, such as for $\tilde{\Delta}_\omega$. In contrast, when Δ_{lsq} is used, the substitution of SMG with $S3QR$ resulted in only minor differences.

For the considered test cases, the present study revealed no distinguishable impact of the proposed techniques on the shielding property of the DDES blending function. However, it should be noted that the present work did not examine in detail the impact of the new approach, up on the near wall RANS region. In those cases with free inflow condition, where the ν_{sgs} is set to around 4 times the molecular kinematic viscosity (classical inflow for Spalart-Allmaras RANS models). This can be the case of any bluff-body, such as circular cylinders or airfoil profiles. Nevertheless, without careful additional testing, beyond the scope of the present work, the shielding capability of the present formulation can not be confirmed.

Acknowledgements

This work has been financially supported by the *Ministerio de Economía y Competitividad*, Spain (No. ENE2017-88697-R). A.P.V. was supported by a *FI-DGR 2016* predoctoral contract (No. 2018FI_B2_00072) financed by *Generalitat de Catalunya*, Spain. F.X.T. was supported by a *Ramón y Cajal* postdoctoral Contract (No. RYC-2012-11996) financed by the *Ministerio de Economía y Competitividad*, Spain. A.D. and A.G. are supported by the Research project 20-02-01 of the Department of the Moscow Center for Fundamental and Applied Mathematics at the Keldysh Institute of Applied Mathematics of Russian Academy of Sciences. The *NOISEtte* computations were carried out using the equipment of the shared research facilities of HPC computing resources at Lomonosov Moscow State University and the computing resources of the federal collective usage center Complex for Simulation and Data Processing for Mega-science Facilities at NRC "Kurchatov Institute", `http://ckp.nrcki.ru/`.

References

[1] Spalart, P. R., Deck, S., Shur, M. L., Squires, K. D., Strelets, M. K., and Travin, A., "A new version of detached-eddy simulation, resistant to ambiguous grid densities," *Theoretical and Computational Fluid Dynamics*, Vol. 20, No. 3, 2006, pp. 181–195.

[2] Spalart, P. R., Jou, W.-H., Strelets, M., and Allmaras, S., "Comments on the Feasibility of LES for Wings, and on a Hybrid RANS/LES Approach," *In 1st AFOSR international conference on DNS/LES*, 1997, pp. 137–147.

[3] Probst, A., Radespiel, R., and Knopp, T., "Detached-Eddy Simulation of Aerodynamic Flows Using a Reynolds-Stress Background Model and Algebraic RANS/LES Sensors," *20th AIAA Computational Fluid Dynamics Conference, Honolulu, Hawaii*, AIAA Paper 2011-3206, American Institute of Aeronautics and Astronautics, 2011.

[4] Knopp, T., and Probst, A., "An algebraic sensor for the rans-les switch in delayed detached-eddy simulation," *New Results in Numerical and Experimental Fluid Mechanics VIII. NNFM*, Vol. 121, edited by A. Dillmann, G. Heller, H. Kreplin, W. Nitsche, and I. Peltzer, 2013, pp. 457–464.

[5] Menter, F., "Stress-Blended Eddy Simulation (SBES) - A New Paradigm in Hybrid RANS-LES Modeling," *Progress in Hybrid RANS-LES Modelling. HRLM 2016. NNFM*, Vol. 137, edited by Y. Hoarau, S. Peng, D. Schwamborn, and A. Revell, 2018, pp. 27–37.

[6] Deck, S., and Renard, N., "Towards an enhanced protection of attached boundary layers in hybrid RANS/LES methods," *Journal of Computational Physics*, Vol. 400, 2020, p. 108970.

[7] Mockett, C., Fuchs, M., Garbaruk, A., Shur, M., Spalart, P., Strelets, M., Thiele, F., and Travin, A., "Two Non-zonal Approaches to Accelerate RANS to LES Transition of Free Shear Layers in DES," *Progress in Hybrid RANS-LES Modelling*, Springer International Publishing, Cham, 2015, pp. 187–201.

[8] Chauvet, N., Deck, S., and Jacquin, L., "Zonal Detached Eddy Simulation of a Controlled Propulsive Jet," *AIAA Journal*, Vol. 45, No. 10, 2007, pp. 2458–2473.

[9] Deck, S., "Recent improvements in the Zonal Detached Eddy Simulation (ZDES) formulation," *Theoretical and Computational Fluid Dynamics*, Vol. 26, 2012, p. 523–550.

[10] Smagorinsky, J., "General circulation experiments with the primitive equations," *Monthly Weather Review*, Vol. 91, No. 3, 1963, pp. 99–164.

[11] Nicoud, F., Toda, H., Cabrit, O., Bose, S., and Lee, J., "Using singular values to build a subgrid-scale model for large eddy simulations," *Physics of Fluids*, Vol. 23, No. 8, 2011, p. 085106.

[12] Fuchs, M., Sesterhenn, J., Thiele, F., and Mockett, C., "Assessment of novel DES approach with enhanced SGS modelling for prediction of separated flow over a delta wing," *22nd AIAA Computational Fluid Dynamics Conference*, 2015.

[13] Probst, A., Schwamborn, D., Garbaruk, A., Guseva, E., Shur, M., Strelets, M., and Travin, A., "Evaluation of grey area mitigation tools within zonal and non-zonal RANS-LES approaches in flows with pressure induced separation," *International Journal of Heat and Fluid Flow*, Vol. 68, 2017, pp. 237–247.

[14] Shur, M. L., Spalart, P. R., Strelets, M. K., and Travin, A. K., "An Enhanced Version of DES with Rapid Transition from RANS to LES in Separated Flows," *Flow, Turbulence and Combustion*, Vol. 95, No. 4, 2015, pp. 709–737.

[15] Guseva, E. K., Garbaruk, A. V., and Strelets, M. K., "Assessment of Delayed DES and Improved Delayed DES Combined with a Shear-Layer-Adapted Subgrid Length-Scale in Separated Flows," *Flow, Turbulence and Combustion*, Vol. 98, No. 2, 2017, pp. 481–502.

[16] Trias, F. X., Folch, D., Gorobets, A., and Oliva, A., "Building proper invariants for eddy-viscosity subgrid-scale models," *Physics of Fluids*, Vol. 27, No. 6, 2015, p. 065103.

[17] Trias, F. X., Gorobets, A., and Oliva, A., "A new subgrid characteristic length for large-eddy simulation," *Physics of Fluids*, Vol. 29, 2017, p. 115109.

[18] Pont-Vílchez, A., Santos, D., Trias, F. X., Duben, A., Revell, A., and Oliva, A., "Assessment of LES techniques for mitigating the Grey Area in DDES models," *8th European Conference for Aeronautics and Aerospace Sciences*, 1-4 July, Madrid, Spain, 2019.

[19] Pont-Vílchez, A., Trias, F. X., Revell, A., and Oliva, A., "Assessment and Comparison of a Recent Kinematic Sensitive Subgrid Length Scale in Hybrid RANS-LES," *Progress in Hybrid RANS-LES Modelling*, edited by Y. Hoarau, S.-H. Peng, D. Schwamborn, A. Revell, and C. Mockett, Springer International Publishing, Cham, 2020, pp. 97–107.

[20] Vogel, J. C., and Eaton, J. K., "Combined Heat Transfer and Fluid Dynamic Measurements Downstream of a Backward-Facing Step," *J. Heat Transfer*, Vol. 107, No. 4, 1985, pp. 922–929.

[21] Pont-Vílchez, A., Trias, F. X., Gorobets, A., and Oliva, A., "Direct numerical simulation of backward-facing step flow at $Re_\tau = 395$ and expansion ratio 2," *Journal of Fluid Mechanics*, Vol. 863, 2019, pp. 341–363.

[22] Shur, M., Spalart, P., and Strelets, M., "Jet noise computation based on enhanced DES formulations accelerating the RANS-to-LES transition in free shear layers," *International Journal of Aeroacoustics*, Vol. 15, No. 6-7, 2016, pp. 595–613.

[23] Fuchs, M., Mockett, C., Shur, M., Strelets, M., and Kok, J., "Single-stream round jet at M = 0.9," *Go4Hybrid: Grey Area Mitigation for Hybrid RANS-LES Methods*, Vol. 134, edited by C. Mockett, W. Haase, and D. Schwamborn, Cham, 2018, pp. 125–137.

[24] Gorobets, A., "Parallel Algorithm of the NOISEtte Code for CFD and CAA Simulations," *Lobachevskii Journal of Mathematics*, Vol. 39, No. 4, 2018, pp. 524–532.

[25] Clark, R. A., Ferziger, J. H., and Reynolds, W. C., "Evaluation of subgrid-scale models using an accurately simulated turbulent flow," *Journal of Fluid Mechanics*, Vol. 91, No. 1, 1979, pp. 1–16.

[26] Spalart, P., and Allmaras, S., "A One-Equation Turbulence Model for Aerodynamic Flows," AIAA Paper 92–0439, American Institute of Aeronautics and Astronautics, 1992.

[27] Mockett, C., Fuchs, M., Thiele, F., Wallin, S., Peng, S., Deck, S., Kok, J., van der Ven, H., Garbaruk, A., Shur, M., Strelets, M., and Travin, A., *Non-zonal approaches for grey area mitigation*, Vol. 134, 2018. doi:10.1007/978-3-319-52995-0_2.

[28] Lau, J. C., Morris, P. J., and Fisher, M. J., "Measurements in subsonic and supersonic free jets using a laser velocimeter," *Journal of Fluid Mechanics*, Vol. 93, No. 1, 1979, pp. 1–27.

[29] Lau, J. C., "Effects of exit Mach number and temperature on mean-flow and turbulence characteristics in round jets," *Journal of Fluid Mechanics*, Vol. 105, No. 1, 1981, pp. 193–218.

[30] Simonich, J., Narayanan, S., Barber, T., and Nishimura, M., "High subsonic jet experiments. I - Aeroacoustic characterization, noise reduction and dimensional scaling effects," *6th Aeroacoustics Conference and Exhibit*, American Institute of Aeronautics and Astronautics, 2000.

[31] Arakeri, V. H., Krothapalli, A., Siddavaram, V., Alkislar, M. B., and Lourenco, L. M., "On the use of microjets to suppress turbulence in a Mach 0.9 axisymmetric jet," *Journal of Fluid Mechanics*, Vol. 490, 2003, pp. 75–98.

[32] Bridges, J., and Wernet, M., "Establishing Consensus Turbulence Statistics for Hot Subsonic Jets," *16th AIAA/CEAS Aeroacoustics Conference*, Aeroacoustics Conferences, American Institute of Aeronautics and Astronautics, 2010.

[33] Shur, M., Spalart, P., and Strelets, M., "LES-based evaluation of a microjet noise reduction concept in static and flight conditions," *Procedia Engineering*, Vol. 6, 2010, pp. 44–53.

[34] Duben, A. P., and Kozubskaya, T. K., "Evaluation of Quasi-One-Dimensional Unstructured Method for Jet Noise Prediction," *AIAA Journal*, Vol. 57, No. 7, 2019, pp. 1–14.

[35] Spalart, P., Shur, M., Strelets, M., and Travin, A., *Sensitivity of Landing-Gear Noise Predictions by Large-Eddy Simulation to Numerics and Resolution*, 2012.

[36] Koobus, B., Alauzet, F., and Dervieux, A., "Numerical algorithms for unstructured meshes," *Computational Fluid Dynamics*, edited by F. Magoules, Progress in Astronautics and Aeronautics, CRC Press, 2011, pp. 131–204.

[37] Abalakin, I., Bakhvalov, P., and Kozubskaya, T., "Edge-based reconstruction schemes for unstructured tetrahedral meshes," *International Journal for Numerical Methods in Fluids*, Vol. 81, No. 6, 2016, pp. 331—-356.

[38] Winant, C. D., and Browand, F. K., "Vortex pairing : The mechanism of turbulent mixing-layer growth at moderate Reynolds number," *Journal of Fluid Mechanics*, Vol. 63, No. 2, 1974, pp. 237–255.